A ubiquitin-proteasome pathway degrades the inner nuclear membrane protein Bqt4 to maintain nuclear membrane homeostasis

Toan Khanh Le[1], Yasuhiro Hirano[1], Haruhiko Asakawa[1], Koji Okamoto[2], Tokuko Haraguchi[1] and Yasushi Hiraoka[1,*]

[1] Nuclear Dynamics Group, Graduate School of Frontier Biosciences, Osaka University, Suita 565-0871, Japan;

[2] Laboratory of Mitochondrial Dynamics, Graduate School of Frontier Biosciences, Osaka University, Suita 565-0871, Japan

Running title: Bqt4 degradation pathway in NE

[*] **Corresponding to:**

Yasushi Hiraoka (hiraoka@fbs.osaka-u.ac.jp), Graduate School of Frontier Biosciences, Osaka University, 1-3 Yamadaoka, Suita 565-0871, Japan. Tel.: +81-6-6879-4621, FAX: +81-6-6789-4622

Keywords: Inner nuclear membrane, Protein degradation, Fission Yeast, Bqt3, Bqt4

Summary statement

The appropriate level of the inner nuclear membrane protein Bqt4 is maintained by ubiquitin-proteasome-mediated degradation. Aberrant accumulation of Bqt4 disturbs the nuclear membrane homeostasis.

Abstract

Aberrant accumulation of inner nuclear membrane (INM) proteins has been associated with deformed nuclear morphology and certain mammalian diseases. However, the mechanisms by which INM homeostasis is maintained remain poorly understood. In this study, we explored the degradation mechanisms of the INM protein Bqt4 in the fission yeast *Schizosaccharomyces pombe*. We have previously shown that Bqt4 interacts with the transmembrane protein Bqt3 at the INM and is degraded in the absence of Bqt3. Here, we revealed that excess Bqt4 unassociated with Bqt3 was targeted for degradation by the ubiquitin-proteasome system localized in the nucleus and that Bqt3 antagonized this process. The degradation process involves the Doa10 E3 ligase complex at the INM. Bqt4 is a tail-anchored protein and extraction from the membrane by the Cdc48 complex is required for its degradation. The C-terminal transmembrane domain of Bqt4 is necessary and sufficient for proteasome-dependent protein degradation. Accumulation of Bqt4 at the INM impaired cell viability with nuclear envelope deformation, suggesting that the quantity control of Bqt4 plays an important role in nuclear membrane homeostasis.

Introduction

The eukaryotic nucleus is enclosed by the nuclear envelope (NE), which separates the nucleoplasm from the cytoplasm. The NE comprises the inner and outer nuclear membranes (INM and ONM, respectively). The ONM is continuous with the endoplasmic reticulum (ER). The INM is involved in the organization and regulation of chromosomes by modulating the chromatin potential for gene expression, DNA replication, DNA damage repair, and genome stability (Mekhail and Moazed, 2010; Hirano et al., 2020a; Pawar and Kutay, 2021). Excess amounts of INM proteins cause aberrant accumulation at the NE, often causing nuclear deformation and malfunctioning (Gonzalez et al., 2012). The aberrant accumulation of INM proteins has been linked to certain mammalian diseases. For example, accumulation of the INM protein SUN1 was found to be pathogenic in human laminopathies, such as Emery-Dreifuss muscular dystrophy and Hutchinson-Gilford progeria syndrome (Chen et al., 2012). Therefore, the amounts of INM protein must be regulated. However, the mechanisms that regulate levels of resident INM proteins to maintain INM homeostasis remain poorly understood.

Mechanisms for ER membrane homeostasis have been well studied: ER membrane proteins are regulated through the ER-associated degradation (ERAD) system, which is involved in degrading misfolded or mislocalized ER proteins as a means of protein quality control (Vembar and Brodsky, 2008; Ruggiano et al., 2014; Christianson and Carvalho, 2022). ERAD involves the ubiquitin-proteasome system (UPS), in which polyubiquitin chains are covalently attached to a substrate protein, leading to its subsequent recognition and degradation by the 26S proteasome complex. Ubiquitination reactions involve three different classes of enzymes: E1 ubiquitin-activating enzymes, E2 ubiquitin-conjugating enzymes, and E3 ubiquitin ligases such as Hrd1 and Doa10 (human MARCHF6/TEB4). INM-associated degradation (INMAD) has been proposed as an extension of ERAD to maintain INM

69 homeostasis, which also depends on the UPS (Foresti et al., 2014; Khmelinskii et al., 2014;
70 Koch and Yu, 2019; Smoyer and Jaspersen, 2019; Mannino and Lusk, 2022). It has been
71 shown that in the budding yeast *Saccharomyces cerevisiae*, ERAD and INMAD require
72 additional machinery for the degradation of integral membrane proteins, involving
73 Cdc48/p97, an ATPase associated with diverse cellular activities (AAA-ATPase), which
74 removes the ubiquitinated proteins from the membrane before transferring them to the
75 proteasome for degradation (Ruggiano et al., 2014; Christianson and Carvalho, 2022; Koch
76 and Yu, 2019; Smoyer and Jaspersen, 2019; Mannino and Lusk, 2022).
77 In the fission yeast *Schizosaccharomyces pombe*, several INM proteins have been
78 studied for their roles in the organization and regulation of chromosome stability, including
79 Ima1, Lem2, Man1, Bqt3, and Bqt4 (Chikashige et al., 2006; Chikashige et al., 2009; Hiraoka
80 et al., 2011; Steglich et al., 2012; Gonzalez et al., 2012; Tange et al., 2016; Hirano et al.,
81 2020b). In particular, we found that Bqt4 was degraded in the absence of Bqt3 (Chikashige et
82 al., 2009). Bqt3 is predicted to be a transmembrane INM protein composed of 7
83 transmembrane domains (TMDs) along its entire length; Bqt4, which interacts with Bqt3, is
84 predicted as a tail-anchored protein (Chikashige et al., 2009). Bqt3 and Bqt4 are required for
85 anchoring telomeres to the NE during vegetative growth and for clustering telomeres to the
86 spindle-pole body through the meiosis-specific telomere-binding proteins, Bqt1 and Bqt2
87 (Chikashige et al., 2006; Chikashige et al., 2009). Importantly, Bqt4 interacts with Lem2
88 (Hirano et al., 2018), and the depletion of Bqt4 is synthetic-lethal with the depletion of Lem2
89 (Tange et al., 2016; Kinuagsa et al., 2019). Therefore, it is expected that Bqt4 plays important
90 roles in cell viability. However, the non-telomeric vital roles of Bqt4 and the mechanisms
91 underlying its degradation remain unknown. In this study, we identified the factors required
92 for Bqt4 degradation via an INM-associated degradation mechanism. We also demonstrated

93 that excess amounts of Bqt4 result in impaired nuclear morphology and growth defects,
94 indicating the importance of regulated degradation of Bqt4 for membrane homeostasis.
95
96 **Results**
97 **INM protein Bqt4 is degraded via the ubiquitin-proteasome system**
98 Because the ubiquitin-proteasome system accounts for the selective degradation of many
99 proteins in the nucleus (Enam et al., 2018; Franić et al., 2021), we first tested the requirement
100 of the proteasome for Bqt4 degradation. We treated cells expressing N-terminally GFP-
101 tagged Bqt4 (GFP-Bqt4) under its own promoter with bortezomib (BZ), a chemical
102 proteasome inhibitor working in *S. pombe* (Takeda et al., 2011), and assessed the
103 fluorescence levels of GFP-Bqt4 at 4 h after drug addition in the presence or absence of Bqt3.
104 As a result of the treatment, GFP-Bqt4 fluorescence in the nucleus of both *bqt3+* and *bqt3*
105 cells was elevated (Figure. 1A). To confirm this result, we checked protein levels by Western
106 blotting, which consistently showed an increase in GFP-Bqt4 protein levels in these strains
107 upon proteasomal inhibition by BZ (Figure. 1B). Notably, the GFP-Bqt4 signal was restored
108 upon proteasome inhibition in the absence of Bqt3, and also elevated even in the presence of
109 Bqt3. This suggests that Bqt4 is constitutively turned over by the proteasome system and its
110 association with Bqt3 antagonizes this process. We sought to confirm this phenomenon by
111 introducing temperature-sensitive *mts2-1* and *mts3-1* proteasome mutations (Gordon and
112 McGurk, 1993; Gordon et al., 1996). Using both fluorescence microscopy and Western
113 blotting, we found that GFP-Bqt4 levels increased in *bqt3*$^{+}$ and *bqt3Δ* cells carrying these
114 proteasome mutations at the restrictive temperature of 36ºC, as compared to the
115 corresponding wild-type strains (Figure. 1C, D; Figure. S1). These results indicate that Bqt4
116 degradation proceeds via the proteasome system.

117 Since proteins are ubiquitinated as a requirement for recognition by the proteasome,
118 we examined whether Bqt4 is modified by polyubiquitination. We immunoprecipitated GFP-
119 Bqt4 under denaturing conditions and detected associated ubiquitin by immunoblotting.
120 Ubiquitinated forms of Bqt4 were detected in *bqt3*Δ cells and were enriched in both *bqt3*$^{+}$
121 and *bqt3*Δ cells when proteasomal activity was inhibited (Figure. 1E), suggesting that Bqt4 is
122 targeted to the proteasome by polyubiquitin modification.
123 Vacuolar autophagy is another pathway through which cells degrade proteins. Thus,
124 we next examined whether Bqt4 degradation is regulated by the vacuolar autophagy pathway
125 by analyzing GFP-Bqt4 levels in *bqt3*Δ cells lacking *isp6* and *atg1* genes. Isp6 is a serine
126 protease necessary for vacuolar function, and Atg1 is a serine/threonine protein kinase that is
127 the upstream initiator of the autophagy machinery. Deletion of these two genes has been
128 shown to completely impair the vacuolar autophagy pathway (Kohda et al., 2007). We found
129 that the deletion of *isp6* and *atg1* had no detectable effect on the quantity of GFP-Bqt4 in the
130 absence of Bqt3, suggesting that Bqt4 degradation does not involve the vacuolar autophagy
131 system (Figure. 1F). Collectively, we concluded that the Bqt4 protein is degraded by the
132 ubiquitin-proteasome system, without involvement of the vacuolar autophagy pathway.
133
134 **Bqt4 degradation occurs in the nucleus**
135 Next, we attempted to determine whether Bqt4 was degraded in the nucleus by the nuclear
136 proteasome. In *S. pombe*, proper targeting of proteasomes to the nucleus requires the
137 tethering factor Cut8 (Tatebe and Yanagida, 2000). In *cut8* mutants, proteasomes fail to
138 localize in the nucleus and become mostly cytoplasmic (Tatebe and Yanagida, 2000).
139 Because nuclear protein degradation depends on the localization of proteasomes in the
140 nucleus (Takeda and Yanagida, 2005), we examined the level of GFP-Bqt4 in *bqt3*$^{+}$ and
141 *bqt3Δ* cells carrying the temperature-sensitive *cut8-563* mutation. We found that GFP-Bqt4

142 degradation was suppressed in *cut8-563* cells shifted to the nonpermissive temperature of
143 36°C (Figure. 2A, B). Taken together, our results strongly suggest that Bqt4 is degraded
144 mainly by the proteasome within the nucleus.
145
146 **Bqt4 degradation involves the Doa10 E3 ligase complex**
147 We next sought to identify the specific E3 ubiquitin ligase that directly recognizes Bqt4. As
148 Bqt4 is a protein associated with the INM, we investigated whether membrane-localized
149 Hrd1 and Doa10 E3 ligases participate in the Bqt4 degradation pathway. Deletion of *doa10*$^{+}$
150 partially restored GFP-Bqt4 levels in the absence of Bqt3, whereas deletion of *hrd1*$^{+}$ did not
151 (Figure. 3A and B, comparing *hrd1*Δ to *doa10*Δ). These results are consistent with previous
152 studies that showed that Doa10 partially localizes to the INM and is involved in the
153 degradation of certain nuclear and INM substrates, whereas Hrd1 is found exclusively in the
154 ER (Deng and Hochstrasser, 2006; Boban et al., 2014). Additionally, the double deletion of
155 *doa10*$^{+}$ and *hrd1*$^{+}$ showed no obvious synthetic effect on GFP-Bqt4 restoration compared to
156 the deletion of *doa10*$^{+}$ alone (Figure. 3A, B). We also checked the quantity of GFP-Bqt4 in
157 mutants lacking Ubc6 and Ubc7, which are E2 ubiquitin-conjugating enzymes associated
158 with Doa10 (Swanson et al., 2001). We found that GFP-Bqt4 levels increased to some extent
159 in *ubc6*Δ, *ubc7*Δ single, and *ubc6*Δ *ubc7*Δ double mutants (Figure. 3C, D). These findings
160 indicate that the Doa10 complex contributes to the degradation of Bqt4 in the INM.
161 Although degradation of Bqt4 depended on Doa10, the level of GFP-Bqt4 was only
162 partially restored in the *doa10*Δ mutant (Figure. 3A, B). Therefore, we attempted to search
163 for other redundant E3 ligases involved in Bqt4 degradation. We constructed mutants of E3
164 ligases and their components that are suggested to localize or function in the ER and nucleus,
165 namely *meu34*Δ, *dsc1*Δ, *ubr1*Δ, *ubr11*Δ, *san1*Δ, *hul5*Δ, *ptr1-1*, and *cut9-665* (PomBase,
166 Matsuyama et al., 2006, Nielsen et al., 2014; Enam et al., 2018; Franić et al., 2021), and

167 observed GFP-Bqt4 fluorescence intensity in these mutants. Except for the *hul5*Δ mutant,
168 which exhibited a slight increase in the GFP-Bqt4 level, the other mutants showed no
169 detectable changes by fluorescence microscopy (Figure. S2). Thus, unidentified E3 ligases
170 appear to function in the INM in cooperation with Doa10 to ubiquitinate Bqt4.
171
172 **Bqt4 is an integral membrane protein**
173 We have previously shown that the Bqt4 protein localizes exclusively to the nucleoplasmic
174 side of the INM, and this localization requires its C-terminal helix (Chikashige et al., 2009).
175 However, as this C-terminal helix is predicted to be a weak candidate for the TMD (Figure.
176 S3), we examined whether Bqt4 is an integral or a peripheral membrane protein to understand
177 how Bqt4 is removed from the INM before degradation. Therefore, we performed a
178 membrane protein extraction experiment. In brief, cells were lysed, treated under various
179 conditions, and then separated into pellet and supernatant fractions by ultracentrifugation,
180 followed by Western blotting; a protein was expected to enter the pellet fraction if it
181 remained in the lumen or associate with the membrane after the treatment. As a control for a
182 luminal and an integral membrane protein, we used GFP-ADEL (Rossanese et al., 2001) and
183 GFP-Bqt3 (Chikashige et al., 2009), respectively. As shown in Figure. 4, all these proteins
184 were extracted from the membrane by treatment with Triton X-100 and 0.5 M NaCl.
185 However, similar to Bqt3, Bqt4 was not dissociated from the membrane by sodium carbonate
186 (pH 11), urea, or NaCl treatments, which can strip peripheral membrane proteins. In contrast,
187 GFP-ADEL was completely released from the membrane by sodium carbonate treatment, as
188 expected for luminal proteins. Thus, Bqt4 is likely to behave as a tail-anchored protein and its
189 C-terminal sequence can act as a TMD that is integrally embedded in the INM.
190
191 **Degradation of Bqt4 requires the Cdc48 retrotranslocation complex**

192 The ATPase Cdc48 has been shown to facilitate the degradation of ubiquitinated ERAD
193 membrane substrates by extracting them from the ER membrane in *S. cerevisiae* (Ye et al.,
194 2001; Jarosch et al., 2002; Rabinovich et al., 2002; Wolf and Stolz, 2012). Therefore, we
195 investigated whether Cdc48 is necessary for Bqt4 degradation. To this end, we generated a
196 *cdc48* mutant bearing mutations in both the D1 (P267L) and D2 (A550T) ATPase domains,
197 based on the temperature-sensitive *cdc48-6* allele in *S. cerevisiae* (Schuberth and Buchberger,
198 2005; Ruggiano et al., 2016) (Figure. 5A). The *cdc48* mutant (*cdc48-P267L/A550T*)
199 exhibited cold-sensitive growth defects (Figure. 5B), suggesting that these mutations
200 impaired Cdc48 activity in *S. pombe*. Inactivation of *cdc48-P267L/A550T* by shifting to the
201 nonpermissive temperature of 16°C elevated the level of GFP-Bqt4 in $bqt3^{+}$ and *bqt3Δ* cells
202 (Figure. 5C, D, Figure. S4). As the ATPase activity of Cdc48 is required for extracting
203 membrane proteins, our results suggest that Bqt4 is extracted from the INM by the Cdc48
204 complex prior to its degradation.
205
206 **The C-terminal TMD of Bqt4 acts as a degradation signal**
207 We previously showed that Bqt4 degradation depends on its C-terminal TMD (residues 414-
208 432) (Chikashige et al., 2009). To identify the minimal region of Bqt4 that is sufficient for its
209 degradation, we performed an analysis of truncated C-terminal fragments based on the
210 structure of Bqt4 predicted by AlphaFold2 (Figure. 6, Figure. S5). The Bqt4 fragment
211 ($Bqt4C^{369-432}$) containing the helix domain and the adjacent intrinsically disordered sequence
212 reproduced behaviors of full-length Bqt4, as shown in Figure. 1A, that is, localization and
213 responses to BZ, both in the presence and absence of Bqt3 (Figure. 6). The helix domain
214 alone ($Bqt4C^{394-432}$) showed weaker localization at the NE and somewhat diffused to the
215 membrane compartments in the cytoplasm; nevertheless, this fragment was degraded in the
216 absence of Bqt3, and its level increased with BZ treatment (Figure. 6). The TMD alone

217 (Bqt4C$^{414-432}$) showed even weaker localization at the NE with diffusion to the cytoplasm, but
218 showed the same responses, that is, degradation in the absence of Bqt3, and increased levels
219 upon BZ treatment (Figure. 6). These results indicate that the C-terminal fragment containing
220 residues 369–432 was necessary and sufficient for the NE localization of Bqt4, and its
221 truncation successively reduced the ability of NE localization. These results also indicated
222 that the C-terminal TMD of Bqt4 is sufficient for its degradation in the absence of Bqt3.
223 To further narrow the TMD of Bqt4 for proteasome-dependent degradation and Bqt3-
224 dependent protection against degradation, we generated constructs with a shorter TMD
225 truncated of the last seven residues (Bqt4C$^{369-425}$ and Bqt4C$^{414-425}$). The fragments Bqt4C^{369-}
226 ^{425} and Bqt4C$^{414-425}$ lost their dependency on Bqt3 for degradation and showed similar
227 behaviors in the presence or absence of Bqt3. While Bqt4C$^{369-425}$ retained slight localization
228 at the NE and Bqt4C$^{414-425}$ showed diffuse localization in the cytoplasm, both fragments
229 showed increased signal levels in the presence of BZ. These fragments, lacking the last seven
230 residues, are also substrates of proteasomal degradation in a Bqt3-independent manner
231 (Figure. 6). These results suggest that the fragment of residues 414–425 is sufficient for
232 proteasomal degradation and that the fragment of residues 426–432 is required for Bqt3-
233 dependent protection against proteasomal degradation.
234
235 **Excess Bqt4 causes deformation of the NE**
236 We observed that inhibition of proteasomal degradation caused striking NE expansion and
237 deformation with irregular protrusions and invaginations, especially in *bqt3*$^{+}$ cells, in which
238 Bqt4 levels were excessively high (Figure. 1A, C). We hypothesized that the high levels of
239 Bqt4 in these cells were responsible for this abnormal NE morphology. To test this
240 possibility, we inhibited proteasomal degradation in the presence or absence of endogenous
241 Bqt4 and visualized the NE using Ish1-GFP as an NE marker, and then nuclear deformation

242 was assessed by roundness of the nucleus. Only when Bqt4 was present was strong
243 deformation of NE observed upon proteasomal inhibition (see *bqt4*$^{+}$+BZ; Figure. 7A),
244 suggesting that Bqt4 was an essential factor causing this phenomenon. To ascertain whether
245 this abnormal phenotype was caused by an accumulation of Bqt4, we overexpressed GFP-
246 Bqt4 under the *nmt1* promoter using YAM2 to control the expression level. YAM2, a
247 chemical compound, suppresses *nmt1* promoter activity depending on its concentration
248 (Nakamura et al., 2011). Overexpression of GFP-Bqt4 at levels similar to proteasomal
249 inhibition reproduced the observed nuclear-deformed morphology, and maximal
250 overexpression of GFP-Bqt4 resulted in even more striking NE proliferation and deformation
251 in both *bqt3*$^{+}$ and *bqt3Δ* cells, indicating that abnormal NE morphology depended on the
252 amount of Bqt4 (Figure. 7B). Taken together, these results support our hypothesis that Bqt4
253 is the only protein whose accumulation upon degradation inhibition induces aberrant nuclear
254 morphology. Finally, we investigated whether excess GFP-Bqt4 was toxic. We found that
255 overproduction of GFP-Bqt4 caused a growth defect in both *bqt3*$^{+}$ and *bqt3Δ* strains
256 compared to cells expressing endogenous levels of Bqt4 (Figure. 7C). Altogether, these
257 observations suggest that Bqt4 plays an important role in regulating NE morphology and that
258 a nuclear proteasomal degradation pathway controlling the quantity of Bqt4 is crucial for
259 nuclear membrane homeostasis.
260

261 **Discussion**

262 In this study, we identified the molecular factors required for the degradation of the INM
263 integral protein Bqt4 in *S. pombe* (Figure. 8). Bqt4 undergoes degradation by an INMAD
264 mechanism involving the Doa10 E3 ligase, which possibly recognizes the C-terminal TMD
265 of Bqt4 as a degron. Subsequently, the AAA-ATPase Cdc48 removes Bqt4 from the INM,
266 and Bqt4 is finally degraded via the nuclear proteasome. We also demonstrated that
267 undegraded Bqt4 accumulating in the INM caused strong deformation of the NE and resulted
268 in growth defects. Bqt4 escapes degradation when interacting with Bqt3 through its C-
269 terminal TMD. Excess amounts of Bqt4 that are unbound to Bqt3 are subjected to INMAD-
270 mediated degradation to avoid the accumulation of Bqt4 at the NE. These findings contribute
271 to our understanding of the significance of INM protein degradation in INM homeostasis.
272

273 **Bqt4 is a native INM degradation substrate containing an intramembrane degron**

274 Studies in mammalian cells have suggested that integral INM proteins are largely stable
275 (Toyama et al., 2013; Buchwalter et al., 2019) and it has been difficult to study their turnover.
276 In the budding yeast *S. cerevisiae*, most of the INMAD substrates characterized thus far are
277 not native INM proteins, but rather nuclear soluble proteins (Swanson et al., 2001; Ravid et
278 al., 2006) and ER membrane proteins that are unassembled or mislocalized to the INM
279 (Foresti et al., 2014; Khmelinskii et al., 2014; Natarajan et al., 2020). Thus, our study of Bqt4
280 provides an opportunity for a native INM substrate to obtain further insight into the
281 mechanisms governing INM protein degradation. Along with several previous studies that
282 reported a handful of native INM substrates (Boban et al., 2014; Pantazopoulou et al., 2016;
283 Smoyer et al., 2019; Koch et al., 2019), our results on the degradation of the INM protein
284 Bqt4 demonstrate that INMAD is responsible for not only maintaining INM identity by

285 removing foreign proteins but also for maintaining the proteostasis of INM integral
286 components.
287 An important question is whether INMAD machinery specifically recognizes its
288 substrates. Although a degradation signal has yet to be identified for integral INM substrates
289 of INM-localized E3 ubiquitin ligases, such as Doa10 and the Asi complex, we identified that
290 Bqt4 has an intramembrane degron. This suggests that INMAD may not simply detect and
291 degrade misfolded or mislocalized proteins at the INM, but instead specifically recognizes a
292 substrate to regulate its protein levels.
293
294 **An INM protein degradation pathway in *S. pombe***
295 In *S. cerevisiae*, the Doa10 E3 ubiquitin ligase cooperates with the Asi complex in INMAD
296 (Koch and Yu, 2019; Smoyer and Jaspersen, 2019; Mannino and Lusk, 2022). As homologs
297 of Asi proteins are absent in *S. pombe* as in other species, INMAD mechanisms may be
298 diverse among organisms. However, increasing evidence has shown that the degradation of
299 INM proteins in plants and mammals also employs the UPS and Cdc48/p97 (Tsai et al., 2016;
300 Huang et al., 2020; Krshnan et al., 2022), raising a general mechanism for INM protein
301 degradation.
302 In *S. cerevisiae*, Doa10 E3 ligase can passively diffuse from the ER to the INM and
303 functions in both ERAD and INMAD (Deng and Hochstrasser, 2006). In particular, Doa10
304 has been implicated in mediating the degradation of the INM protein Asi2, which itself is a
305 component of INMAD (Boban et al., 2014). In *S. pombe*, Bqt4 degradation also depends on
306 Doa10, indicating that Bqt4 is subject to regulation by INMAD. In addition, our data indicate
307 that *S. pombe* might possess additional unidentified redundant E3 ligases cooperating with
308 Doa10 at the INM. Because Bqt4 is supposed to be recognized by these E3 ligases at its
309 transmembrane degron, it is expected that the unidentified E3 ligases also localize to the INM

310 membranes ("X(E3)" in Figure 8). Similar situations, in which unidentified E3 ligases
311 degrade an INM substrate, have been reported in *S. cerevisiae* (Pantazopoulou et al. 2016).
312 Likewise, INM-localized E3 ligases have yet to be identified in higher eukaryotes. We
313 speculate that the uncharacterized E3 ligases functioning at the INM in *S. pombe* might
314 operate with E2 ubiquitin-conjugating enzymes other than Ubc6 and Ubc7 because
315 degradation of Bqt4 exhibits limited dependence on these enzymes. Thus, it would be of
316 great interest to identify and characterize other E3 ligases and E2 conjugating enzymes that
317 mediate protein degradation at the INM.
318 The Cdc48 complex plays a central role in the ERAD degradation of ER integral
319 membrane proteins by exerting a pulling force on the ubiquitinated membrane protein via its
320 ATPase activity (Braun, 2002; Rabinovich et al., 2002; Wolf and Stolz, 2012; Bodnar and
321 Rapoport, 2017). Cdc48 has also been implicated in the degradation of the INM proteins Asi1
322 and Msp3 in *S. cerevisiae* (Pantazopoulou et al. 2016; Koch et al., 2019). In *S. pombe*, Cdc48
323 mutations at its ATPase active center impair Bqt4 degradation, indicating that
324 ERAD/INMAD degradation also utilizes the Cdc48 complex to extract membrane-embedded
325 substrates and deliver them to the proteasome for proteolysis. Thus, our study demonstrated
326 the presence of a conserved INMAD system in *S. pombe*.
327
328 **The biological significance of Bqt4 degradation**
329 The INM protein Bqt4 has been suggested to have non-telomeric functions that are currently
330 unknown, yet vital for cell growth, as double deletion of Bqt4 and Lem2 results in synthetic
331 lethality (Tange et al., 2016; Hirano et al., 2018; Kinugasa et al., 2019). In cells lacking both
332 Bqt4 and Lem2, nuclear envelope rupture occurs in association with the leakage of nuclear
333 proteins into the cytoplasm, suggesting that Bqt4, in cooperation with Lem2, plays essential
334 roles in maintaining nuclear membrane integrity (Kinugasa et al., 2019). The nuclear

335 membrane rupture phenotype can be rescued by an increased expression of Elo2, a fatty acid
336 elongase that catalyzes the synthesis of very-long-chain fatty acids (Kinugasa et al., 2019). In
337 addition, depletion of Bqt4 and Lem2 also leads to a reduction in the quantity of t20:0/24:0
338 phytoceramide, the most abundant ceramide species in *S. pombe*, and this reduction can be
339 prevented by the overexpression of Elo2 (Kinugasa et al., 2019). These findings strongly
340 suggest that Bqt4 is involved in nuclear membrane lipid metabolism. Thus, we propose that
341 abnormal accumulation of Bqt4 at the INM may result in excessive lipid synthesis, ultimately
342 leading to nuclear membrane expansion and deformation. One possibility is that Bqt4
343 promotes the synthesis of phospholipids, a major component of the nuclear membrane.
344 Several lines of evidence suggest that increased phospholipid synthesis from phosphatidic
345 acid induces striking NE membrane deformation (Santos-Rosa et al., 2005; Barbosa et al.,
346 2015). The exact mechanisms leading to the deformed nuclear morphology upon the
347 accumulation of Bqt4 remain to be elucidated. Further investigations will advance our
348 understanding of the role of INM protein degradation in the maintenance of nuclear
349 membrane homeostasis.
350
351

352 **Materials and methods**

353 **Yeast strains and culture media**

354 All *S. pombe* strains used in this study are listed in Table S1. Unless otherwise specified, all
355 *S. pombe* strains were cultured in yeast extract with supplements (YES) medium. Malt extract
356 medium (ME) was used to induce sporulation. G418 disulfate (Nacalai Tesque, Japan),
357 Hygromycin B (Wako, Japan), nourseothricin sulfate (Werner BioAgents, Germany), and
358 Blasticidin S (Wako, Japan) were used at concentrations of 100, 200, 100, and 100 μg/ml,
359 respectively, to select strains bearing the respective selection marker.

360

361 **Construction of plasmids and strains**

362 All plasmids were constructed using the NEBuilder system (New England BioLabs, MA,
363 USA) and enzymatic digestion and ligation (TaKaRa, Japan) systems, according to the
364 manufacturer's instructions. Gene disruption and GFP tagging were performed using the
365 direct chromosomal integration method (Wach, 1996; Bähler et al., 1998). The integration
366 cassettes were amplified using a two-step PCR. In the first PCR, fragments (~500 bp
367 genomic regions upstream and downstream of the gene of interest) were amplified from the
368 wild-type *S. pombe* genome using the KOD One DNA polymerase (TaKaRa Bio Inc., Japan).
369 The first PCR products were used as primers in the second step of the PCR to amplify a
370 cassette for integration, which contained a selection marker. For gene disruption, pFA6-
371 kanMX6 (Bähler et al., 1998), pCR2.1-hph, pCR2.1-bsd, and pCR2.1-nat (Sato et al., 2005)
372 were used to generate the integration cassettes. For GFP tagging, pFA6-GFP(S65T)-kanMX6
373 (Bähler et al., 1998) was used to generate the GFP-containing integration cassettes. The
374 cassettes were then transformed into *S. pombe* cells and the desired integrant strains were
375 selected on YES plates containing the appropriate selection agent. Correct disruptions and

376 integrations were confirmed by genomic PCR at the 5′ and 3′ ends using KOD FX Neo
377 (TaKaRa Bio Inc., Japan).
378
379 **Fluorescence microscopy**
380 Fluorescence microscopy data of intracellular GFP fusion proteins in living cells were
381 collected using a DeltaVision microscope system (GE Healthcare Inc., USA) equipped with a
382 pco.edge 4.2 sCMOS camera (PCO, Germany) and a ×60 PlanApo N OSC oil-immersion
383 objective lens (numerical aperture NA=1.4, Olympus, Japan). For live-cell imaging, cells
384 were precultured from a fresh colony, followed by culturing in YES medium at 30°C to reach
385 the logarithmic growth phase (5-10×10^6 cells/ml). The cells were then attached to glass-
386 bottomed culture dishes coated with soybean lectin (Sigma-Aldrich, USA), covered with
387 Edinburgh minimal medium with glutamate (EMMG) medium, and observed at specified
388 temperatures.
389
390 **Image quantification and processing**
391 An identical fluorescence intensity range was applied to all images presented in each panel
392 using the Fiji software (Schindelin et al., 2012).
393 To quantify the fluorescence intensity in the nucleus, we used Fiji software. First, we
394 generated the sum projection image from the raw z-stack images and then subtracted the
395 background signal from the entire image by measuring the mean intensity of a region where
396 no cells exist. Second, the nuclear region was manually or semi-automatically selected. For
397 semi-automatic selection, individual nuclei were selected (original image), and the selected
398 image was blurred using Gaussian blur (blurred image). An appropriate sigma value was
399 applied depending on the image contrast. By subtracting the blurred image from the original
400 image, an edge-enhanced image was generated. The nuclear region was thresholded using the

401 appropriate minimum and maximum intensity ranges. Third, the threshold region was applied
402 to the original image and the total fluorescence intensity of the region was quantified. The
403 nuclear intensities obtained from *bqt3*$^{+}$ cells were averaged and the values were used to
404 calculate the relative fluorescence intensity. The relative fluorescence intensities were
405 plotted, and the results are presented as the mean ± standard deviation.
406 For the roundness index measurement, after selecting individual nuclei, the nuclear
407 membrane signal was thresholded using the appropriate fluorescence intensity ranges. The
408 nuclear region was filled in, and the roundness index was measured using the built-in
409 function in Fiji.
410
411 **Western blotting**
412 Cells were precultured in YES medium at 30°C overnight, inoculated in fresh YES, and then
413 cultured until the cell concentration reached the mid-log phase (5-10×10^6 cells/ml).
414 Approximately 5×10^7 cells were harvested by centrifugation at 4°C, and the cell pellet was
415 washed with 1 ml ice-cold water containing 1 mM phenylmethylsulfonyl fluoride (PMSF).
416 Cells were lysed in 150 µl of ice-cold 1.85 M NaOH containing 7.5% β-mercaptoethanol (β-
417 ME) on ice for 15 min, followed by the addition of 150 µl of ice-cold 55% (v/v)
418 trichloroacetic acid (TCA) to precipitate the proteins, incubation on ice for 15 min, and
419 centrifugation (10 min, 14,000 ×g, 4°C). The protein pellet was then washed twice with ice-
420 cold acetone and dissolved in sample solubilization buffer [50 mM Tris-HCl pH 8.0, 1%
421 SDS, 1× Protease Inhibitor Cocktail (P8215, Sigma-Aldrich, USA), 1 mM PMSF, 1 mM
422 bortezomib]. Total protein concentrations were determined using the BCA assay (Thermo
423 Fisher Scientific, USA) according to the manufacturer's protocol. The samples were further
424 diluted in 2× Laemmli SDS sample buffer to a concentration of 1 µg/µl. After the addition of
425 dithiothreitol to a concentration of 50 mM, samples were heated at 95°C for 10 min before

426 immunoblotting. Identical amounts of protein (10 μg) were separated by SDS–PAGE and
427 transferred to a polyvinylidene difluoride membrane. The membranes were blocked for 1 h at
428 room temperature (approximately 26-28°C) in blocking solution PBST (10 mM Na_2HPO_4,
429 137 mM NaCl, 2.7 mM KCl, 1.76 mM KH_2PO_4, and 0.1% Tween 20) containing 5% skim
430 milk (Nacalai Tesque, Japan). To detect the GFP fusion proteins and β-actin as a loading
431 control, the membranes were probed with anti-GFP rabbit polyclonal antibody (Rockland,
432 USA; 1:2,000 dilution) or anti-β-actin mouse monoclonal antibody (Abcam, UK; 1:2,000
433 dilution) in blocking solution overnight at 4°C. After three rounds of washing with PBST, the
434 membranes were incubated with the appropriate horseradish peroxidase-conjugated
435 secondary antibodies (1:2,000 dilution, Cytiva, USA) in a blocking solution at room
436 temperature for 2 h. After three rounds of washing with PBST, immunoreactive bands were
437 detected using a chemiluminescence system (ImmunoStar LD, Wako, Japan) in a ChemiDoc
438 imaging system (Bio-Rad, USA).
439
440 **Proteasome inhibition**
441 Cells were grown in YES medium to the early mid-log phase (2-5×10^6 cells/ml), as described
442 above. The culture was then divided into two, and the proteasome inhibitor bortezomib (LC
443 Laboratories, USA) dissolved in dimethyl sulfoxide (DMSO) was added to one culture to a
444 final concentration of 1 mM, and the same amount of DMSO was added to the other culture.
445 Cells were incubated at 26°C for 4 h before harvesting for fluorescence microscopy or
446 immunoblotting.
447
448 **Temperature sensitive mutant experiments**
449 For the temperature-sensitive mutant experiments, cells harboring *ts* or *cs* mutations were
450 grown in YES medium to the early mid-log phase (2-5×10^6 cells/ml) at 26°C and 33°C,

451 respectively. The culture temperature was shifted up to 36°C or down to 16°C, and then the
452 cells were incubated for 4 h and 15 h before harvesting, respectively.
453
454 **Ubiquitination detection assay**
455 The ubiquitination detection assay was performed as described previously (Boban et al.,
456 2014) with modifications. Cells were grown in YES medium at 30°C until the mid-log phase
457 (5-10×10^6 cells/ml), and approximately 5×10^8 cells were harvested by centrifugation at 4°C.
458 Where indicated, the proteasome inhibitor bortezomib was added to a final concentration of 1
459 mM for 4 h before the cells were collected. The same volume of DMSO was added to the
460 control samples. The cells were washed with cold water containing 1 mM PMSF and lysed in
461 250 µl of 1.85 N NaOH solution containing 7.5% β-ME for 15 min on ice. Subsequently, the
462 proteins were precipitated by adding 250 µl of 55% (v/v) TCA, followed by incubation for 15
463 min on ice. The proteins were pelleted by centrifugation (10 min, 14,000 ×g, 4°C) and
464 washed with 500 µl of 50 mM Tris before being dissolved in 200 µl denaturation solution [25
465 mM Tris-HCl pH 7.4, 2% SDS, 2 mM ethylenediaminetetraacetic acid (EDTA), 1× Protease
466 Inhibitor Cocktail (P8215, Sigma-Aldrich, USA), 1 mM PMSF, 1 mM bortezomib, 10 µM
467 PR-619 (SML0430, Sigma-Aldrich, USA), and 50 mM 2-chloroacetamide (032-09762, Fuji
468 film Wako, Japan)]. Total protein concentrations were determined using the BCA assay
469 (Thermo Fisher Scientific, USA) according to the manufacturer's protocol. The samples were
470 incubated at 65°C for 10 min and clarified by centrifugation (5 min, 15,000 ×g, room
471 temperature). Equal amounts of protein lysates were diluted five-fold with cold IP dilution
472 buffer (50 mM Tris-HCl pH 7.5, 1.2% Triton X-100, 2 mM EDTA, 100 mM NaCl, 1 ×
473 Protease Inhibitor Cocktail (P8215, Sigma-Aldrich, USA), 1 mM PMSF, 1 mM bortezomib,
474 10 µM PR-619, and 50 mM 2-chloroacetamide), incubated with gentle rotation at 4°C for 1 h,
475 and cleared by centrifugation at 14,000 ×g for 10 min. A portion (20 µl) of the sample (2%

476 input) was mixed with 2× Laemmli SDS sample buffer (20 µl) and frozen until analysis. The
477 remaining sample was mixed with antibody-coupled beads prepared from 2 µg anti-GFP
478 rabbit polyclonal antibody (Rockland) and 50 µl Protein-A-coupled Dynabeads (Life
479 Technologies, USA) according to the manufacturer's instructions. The samples were
480 immunoprecipitated at 4°C for 3 h with gentle rotation and pelleted using a magnet. The
481 pellets were then washed as follows: twice with washing solution A (50 mM Tris-HCl pH
482 7.4, 2 mM EDTA, 100 mM NaCl, 1% Triton X-100, 0.4% SDS), once with washing solution
483 B (50 mM Tris-HCl pH 7.4, 2 mM EDTA, 350 mM NaCl, 1% Triton X-100) including a 10-
484 min incubation at 4°C with gentle rotation, and finally once with washing solution A. To
485 elute the immunoprecipitated protein, 50 µl of 1× Laemmli SDS sample buffer was added to
486 the pellet, and the mixture was incubated for 10 min at 65°C. Ten microliters of each sample
487 were separated on SDS-PAGE gels (8%). For the analysis of immunoprecipitated GFP-Bqt4,
488 the eluate was diluted 1:20 with 1× Laemmli SDS sample buffer. Immunoblotting analysis
489 was performed using an anti-GFP mouse monoclonal antibody (JL8; 1:1000; TaKaRa Bio
490 Inc., Japan) and an anti-ubiquitin mouse monoclonal antibody (P4D1, 1:1000; Santa Cruz
491 Biotechnology, USA). Protein levels in the input samples were assessed using an anti-β-actin
492 antibody (1:2000; Abcam).
493
494 **Membrane association assay**
495 The membrane association assay was performed according to a previously published protocol
496 (Habeck et al., 2015) with slight modifications. *S. pombe* cells expressing GFP-Bqt4 and
497 control proteins (GFP-Bqt3 and GFP-ADEL) were grown to the mid-log phase and mixed at
498 a 1:1:1 ratio before cell harvesting by centrifugation at 4°C. The harvested cells (~5×10^8
499 cells) were washed with cold water containing 1 mM PMSF and resuspended in 500 µl cold
500 fractionation buffer (FB; 0.7 M sorbitol, 50 mM Tris-HCl pH 7.4, 1× Protease Inhibitor

501 Cocktail, 1mM PMSF, 1 mM bortezomib). Resuspended cells were lysed using a bead
502 shocker (2,700 rpm for 10 cycles of 60 s on and 60 s off; Yasui Kikai, Co., Japan), followed
503 by washing the beads three times with 200 µl FB. The cell extracts were combined and debris
504 was removed by centrifugation (600 ×g for 5 min at 4°C). The lysate was divided into five
505 separate aliquots that were subjected to one of the following treatments: (1) FB alone; (2) 0.1
506 M Na_2CO_3, pH 11; (3) 2.5 M urea; (4) 0.5 M NaCl; or (5) 1% Triton X-100 and 0.5 M NaCl.
507 After incubation for 1 h on ice with occasional mixing, the samples were separated into pellet
508 (P) and supernatant (S) fractions by ultracentrifugation at 50,000 ×g for 45 min at 4°C. The
509 pellets were washed once with appropriate supplemented FB by centrifugation (50,000 ×g for
510 45 min at 4°C) before being resuspended in FB. Proteins were then precipitated from the
511 pellet and supernatant fractions by adding 150 µl of 55% (v/v) TCA. After 15 min of
512 incubation on ice, the proteins were pelleted by centrifugation (16,000 ×g for 10 min at 4°C),
513 washed twice with ice-cold acetone, and dissolved in dye-free 2× Laemmli SDS sample
514 buffer. Total protein concentrations were measured using the BCA assay, as described above.
515 The samples were incubated for 10 min at 95°C before immunoblotting.
516
517 **Spot assay**
518 Cells expressing GFP-Bqt4 under the control (*bqt4p*) or nmt1 promoter (*nmt1p*) were
519 precultured in YES medium overnight. Five-fold dilution series of the cells (starting
520 concentration was 8.0×10^5 /mL) were spotted on the EMMG medium plates supplemented
521 with or without 10 µM thiamine, and then the plates were incubated at 30°C for 4 days.
522 For the temperature-sensitivity growth assay, wild-type and Cdc48 mutant cells were
523 spotted in a five-fold dilution series and incubated at 16, 20, 26, 30, 33 and 37°C for 3-6
524 days.
525

Acknowledgements

We thank Chizuru Ohtsuki and Yoshino Kubota for their technical assistance; We also thank to Professor Mitsuhiro Yanagida (OIST) and the National BioResource Project Yeast in Japan for providing the *S. pombe* strains.

Competing interests

The authors declare no competing financial or non-financial interests.

Funding

This study was supported by JSPS KAKENHI Grant Numbers JP20H05891 (to Y. Hirano), JP19H03222 and JP20H05324 (to K.O.), JP18H05528 (to T.H.), and JP18H05533, JP19K22389, and JP20H00454 (to Y. Hiraoka)).

Data availability

Further information and requests for resources and reagents should be directed to Yasushi Hiraoka (hiraoka@fbs.osaka-u.ac.jp)

References

Asakawa, H., Hirano, Y., Shindo, T., Haraguchi, T., Hiraoka, Y. (2022). Fission yeast Ish1 and Les1 interact with each other in the lumen of the nuclear envelope. *Genes Cells* **27**, 643–656. doi: 10.1111/gtc.12981

Barbosa, A.D., Sembongi, H., Su, W.-M., Abreu, S., Reggiori, F., Carman, G.M., Siniossoglou, S. (2015). Lipid partitioning at the nuclear envelope controls membrane biogenesis. *Mol. Biol. Cell* **26**, 3641–3657. doi: 10.1091/mbc.E15-03-0173

Bähler, J., J.Q. Wu, M.S. Longtine, N.G. Shah, A. McKenzie, A.B. Steever, A. Wach, P. Philippsen, and J.R. Pringle. (1998). Heterologous modules for efficient and versatile PCR-based gene targeting in *Schizosaccharomyces pombe*. *Yeast*. 14, 943-951. doi: 10.1002/(SICI)1097-0061(199807)14:10<943::AID-YEA292>3.0.CO;2-Y

Boban, M., Pantazopoulou, M., Schick, A., Ljungdahl, P.O., Foisner, R. (2014). A nuclear ubiquitin-proteasomal pathway targets inner nuclear membrane protein Asi2 for degradation. *J. Cell Sci.* **127**, 3603-3613. doi: 10.1242/jcs.153163

Bodnar N.O., Rapoport T.A. (2017). Molecular Mechanism of Substrate Processing by the Cdc48 ATPase Complex. *Cell* **169**, 722-735. doi: 10.1016/j.cell.2017.04.020

Braun, S., Matuschewski, K., Rape, M., Thoms, S., Jentsch S. (2002). Role of the ubiquitin-selective $CDC48^{UFD1/NPL4}$ chaperone (segregase) in ERAD of OLE1 and other substrates. *EMBO J.* **15**, 615-621. doi: 10.1093/emboj/21.4.615

Buchwalter, A., Schulte, R., Tsai, H., Capitanio, J., Hetzer, M. (2019). Selective clearance of the inner nuclear membrane protein emerin by vesicular transport during ER stress. *eLife* **8**, e49796. doi: 10.7554/eLife.49796

Chen, C.-Y., Chi, Y.-H., Mutalif, R.A., Starost, M.F., Myers, T.G., Anderson, S.A., Stewart, C.L., Jeang, K.-T. (2012). Accumulation of the Inner Nuclear Envelope Protein Sun1 Is Pathogenic in Progeric and Dystrophic Laminopathies. *Cell* **149**, 565–577. doi: 10.1016/j.cell.2012.01.059

Chikashige, Y., Tsutsumi, C., Yamane, M., Okamasa, K., Haraguchi, T., Hiraoka, Y., 2006. Meiotic Proteins Bqt1 and Bqt2 Tether Telomeres to Form the Bouquet Arrangement of Chromosomes. Cell 125, 59–69. doi: /10.1016/j.cell.2006.01.048

Chikashige, Y., Yamane, M., Okamasa, K., Tsutsumi, C., Kojidani, T., Sato, M., Haraguchi, T., Hiraoka, Y. (2009). Membrane proteins Bqt3 and -4 anchor telomeres to the nuclear envelope to ensure chromosomal bouquet formation. *J. Cell Biol.* **187**, 413–427. doi: 10.1083/jcb.200902122

Christianson, J.C., Carvalho, P. (2022). Order through destruction: how ER-associated protein degradation contributes to organelle homeostasis. *EMBO J.* **41**, e109845 doi: 10.15252/embj.2021109845

Deng, M., Hochstrasser, M. (2006). Spatially regulated ubiquitin ligation by an ER/nuclear membrane ligase. *Nature* **443**, 827–831. doi: 10.1038/nature05170

582 Enam, C., Geffen, Y., Ravid, T., Gardner, R.G. (2018). Protein Quality Control Degradation
583 in the Nucleus. *Annu. Rev. Biochem.* **87**, 725–749. doi: 10.1146/annurev-biochem-
584 062917-012730

585 Foresti, O., Rodriguez-Vaello, V., Funaya, C., Carvalho, P. (2014). Quality control of inner
586 nuclear membrane proteins by the Asi complex. *Science* **346**, 751–755. doi:
587 10.1126/science.1255638

588 Franić, D., Zubčić, K., Boban, M. (2021). Nuclear Ubiquitin-Proteasome Pathways in
589 Proteostasis Maintenance. *Biomolecules* **11**, 54. doi: 10.3390/biom11010054

590 Gonzalez, Y., Saito, A., Sazer, S. (2012). Fission yeast Lem2 and Man1 perform fundamental
591 functions of the animal cell nuclear lamina. *Nucleus* **3**, 60–76. doi: 10.4161/nucl.18824

592 Gordon, C., McGurk, G., Dillon, P., Rosen, C., Hastie, N.D. (1993). Defective mitosis due to
593 a mutation in the gene for a fission yeast 265 protease subunit. *Nature* **366**, 355-357. doi:
594 10.1038/366355a0

595 Gordon, C., McGurk, G., Wallace, M., Hastie, N.D., 1996. A Conditional Lethal Mutant in
596 the Fission Yeast 26 S Protease Subunit *mts3*$^{+}$ Is Defective in Metaphase to Anaphase
597 Transition. *J. Biol. Chem.* **271**, 5704–5711. doi: 10.1074/jbc.271.10.5704

598 Habeck, G., Ebner, F.A., Shimada-Kreft, H., Kreft, S.G. (2015). The yeast ERAD-C
599 ubiquitin ligase Doa10 recognizes an intramembrane degron. *J. Cell Biol.* **209**, 261–273.
600 doi: 10.1083/jcb.201408088

601 Hirano, Y., Asakawa, H., Sakuno, T., Haraguchi, T., Hiraoka, Y. (2020a). Nuclear Envelope
602 Proteins Modulating the Heterochromatin Formation and Functions in Fission Yeast.
603 *Cells* **9**, 1908. doi: 10.3390/cells9081908

604 Hirano, Y., Y. Kinugasa, H. Osakada, T. Shindo, Y. Kubota, S. Shibata, T. Haraguchi, and Y.
605 Hiraoka. (2020b). Lem2 and Lnp1 maintain the membrane boundary between the nuclear
606 envelope and endoplasmic reticulum. *Commun. Biol*. **3**, 276. doi: 10.1038/s42003-020-
607 0999-9

608 Hirano, Y., Kinugasa, Y., Asakawa, H., Chikashige, Y., Obuse, C., Haraguchi, T., Hiraoka,
609 Y. (2018). Lem2 is retained at the nuclear envelope through its interaction with Bqt4 in
610 fission yeast. *Genes Cells* **23**, 122–135. doi: 10.1111/gtc.12557

611 Hiraoka, Y., Maekawa, H., Asakawa, H., Chikashige, Y., Kojidani, T., Osakada, H.,
612 Matsuda, A., Haraguchi, T. (2011). Inner nuclear membrane protein Ima1 is dispensable
613 for intranuclear positioning of centromeres: *S. pombe* inner nuclear membrane proteins.
614 *Genes Cells* **16**, 1000–1011. doi: 10.1111/j.1365-2443.2011.01544.x

615 Huang, A., Tang, Y., Shi, X., Jia, M., Zhu, J., Yan, X., Chen, H., Gu, Y. (2020). Proximity
616 labeling proteomics reveals critical regulators for inner nuclear membrane protein
617 degradation in plants. *Nat. Commun.* **11**, 3284. doi: 10.1038/s41467-020-16744-1

618 Jarosch, E., Taxis, C., Volkwein, C., Bordallo, J., Finley, D., Wolf, D.H., Sommer, T. (2002).
619 Protein dislocation from the ER requires polyubiquitination and the AAA-ATPase
620 Cdc48. *Nat. Cell Biol.* **4**, 134–139. doi: 10.1038/ncb746

621 Khmelinskii, A., Blaszczak, E., Pantazopoulou, M., Fischer, B., Omnus, D.J., Le Dez, G.,
622 Brossard, A., Gunnarsson, A., Barry, J.D., Meurer, M., Kirrmaier, D., Boone, C., Huber,
623 W., Rabut, G., Ljungdahl, P.O., Knop, M. (2014). Protein quality control at the inner
624 nuclear membrane. *Nature* **516**, 410–413. doi: 10.1038/nature14096

625 Kinuagsa, Y., Hirano, Y., Sawai, M., Ohno, Y., Shindo, T., Asakawa, H., Chikashige, Y.,
626 Shibata, S., Kihara, A., Haraguchi, T., Hiraoka, Y. (2019). The very-long-chain fatty
627 acid elongase Elo2 rescues lethal defects associated with loss of the nuclear barrier
628 function. *J. Cell Sci.* jcs.229021. doi: 10.1242/jcs.229021

629 Koch, B., Yu, H.-G. (2019). Regulation of inner nuclear membrane associated protein
630 degradation. *Nucleus* 10, 169–180. doi: /10.1080/19491034.2019.1644593

631 Koch, B.A., Jin, H., Tomko, R.J., Yu, H.-G., 2019. The anaphase-promoting complex
632 regulates the degradation of the inner nuclear membrane protein Mps3. *J. Cell Biol.* **218**,
633 839–854. doi: 10.1083/jcb.201808024

634 Kohda, T.A., Tanaka, K., Konomi, M., Sato, M., Osumi, M., Yamamoto, M. (2007). Fission
635 yeast autophagy induced by nitrogen starvation generates a nitrogen source that drives
636 adaptation processes. *Genes Cells* **12**, 155–170. doi: 10.1111/j.1365-2443.2007.01041.x

637 Krshnan, L., Siu, W.S., Van de Weijer, M., Hayward, D., Guerrero, E.N., Gruneberg, U.,
638 Carvalho, P. (2022). Regulated degradation of the inner nuclear membrane protein SUN2
639 maintains nuclear envelope architecture and function. *eLife* **11**, e81573. doi:
640 10.7554/eLife.81573.

641 Lord, S.J., K.B. Velle, R.D. Mullins, and L.K. Fritz-Laylin. (2020). SuperPlots:
642 Communicating reproducibility and variability in cell biology. *J. Cell Biol*. **219**,
643 e202001064. doi: 10.1083/jcb.202001064

644 Mannino, P.J., Lusk, C.P. (2022). Quality control mechanisms that protect nuclear envelope
645 identity and function. *J. Cell Biol.* **221**, e202205123. doi: 10.1083/jcb.202205123

646 Matsuyama, A., Arai, R., Yashiroda, Y., Shirai, A., Kamata, A., Sekido, S., Kobayashi, Y.,
647 Hashimoto, A., Hamamoto, M., Hiraoka, Y., Horinouchi, S., Yoshida, M., 2006.
648 ORFeome cloning and global analysis of protein localization in the fission yeast
649 Schizosaccharomyces pombe. *Nat. Biotechnol.* **24**, 841–847. doi: 10.1038/nbt1222

650 Mekhail, K., Moazed, D. (2010). The nuclear envelope in genome organization, expression
651 and stability. *Nat. Rev. Mol. Cell Biol.* **11**, 317–328. doi: 10.1038/nrm2894

652 Nakamura, Y., Arai, A., Takebe, Y., Masuda, M. (2011). A chemical compound for
653 controlled expression of nmt1-driven gene in the fission yeast *Schizosaccharomyces*
654 *pombe*. *Anal. Biochem.* **412**, 159–164. doi: 10.1016/j.ab.2011.01.039

655 Natarajan, N., Foresti, O., Wendrich, K., Stein, A., Carvalho, P. (2020). Quality Control of
656 Protein Complex Assembly by a Transmembrane Recognition Factor. *Mol. Cell* **77**, 108-
657 119. doi: 10.1016/j.molcel.2019.10.003

658 Nielsen, S., Poulsen, E., Rebula, C., Hartmann-Petersen, R., 2014. Protein Quality Control in
659 the Nucleus. *Biomolecules* **4**, 646–661. doi: 10.3390/biom4030646

660 Pantazopoulou, M., Boban, M., Foisner, R., Ljungdahl, P.O. (2016). Cdc48 and Ubx1
661 participate in an inner nuclear membrane associated degradation pathway that governs
662 the turnover of Asi1. *J. Cell Sci.* **129**, 3770-3780. doi: 10.1242/jcs.189332

663 Pawar, S., Kutay, U. (2021). The Diverse Cellular Functions of Inner Nuclear Membrane
664 Proteins. *Cold Spring Harb. Perspect. Biol.* **13**, a040477. doi:
665 10.1101/cshperspect.a040477

666 Rabinovich, E., Kerem, A., Fröhlich, K.-U., Diamant, N., Bar-Nun, S. (2002). AAA-ATPase
667 p97/Cdc48p, a Cytosolic Chaperone Required for Endoplasmic Reticulum-Associated
668 Protein Degradation. *Mol. Cell. Biol.* **22**, 626–634. doi: 10.1128/MCB.22.2.626-
669 634.2002

670 Ravid, T., Kreft, S.G., Hochstrasser, M. (2006). Membrane and soluble substrates of the
671 Doa10 ubiquitin ligase are degraded by distinct pathways. *EMBO J.* **25**, 533–543. doi:
672 10.1038/sj.emboj.7600946

673 Rossanese, O.W., Reinke, C.A., Bevis, B.J., Hammond, A.T., Sears, I.B., O'Connor, J.,
674 Glick, B.S. (2001). A Role for Actin, Cdc1p, and Myo2p in the Inheritance of Late Golgi
675 Elements in *Saccharomyces cerevisiae*. *J. Cell Biol.* **153**, 47–62. doi:
676 10.1083/jcb.153.1.47

677 Ruggiano, A., Foresti, O., Carvalho, P. (2014). ER-associated degradation: Protein quality
678 control and beyond. *J. Cell Biol.* **204**, 869–879. doi: 10.1083/jcb.201312042

679 Ruggiano, A., Mora, G., Carvalho, P. (2016). Spatial control of lipid droplet proteins by the
680 ERAD ubiquitin ligase Doa10. *EMBO J.* **35**,1644-1655. doi: 10.15252/embj.201593106

681 Santos-Rosa, H., Leung, J., Grimsey, N., Peak-Chew, S., Siniossoglou, S. (2005). The yeast
682 lipin Smp2 couples phospholipid biosynthesis to nuclear membrane growth. *EMBO J.*
683 **24**, 1931–1941. doi: 10.1038/sj.emboj.7600672

684 Sato, M., Dhut, S., Toda, T. (2005). New drug-resistant cassettes for gene disruption and
685 epitope tagging in *Schizosaccharomyces pombe*. *Yeast*. **22**, 583-591. doi:
686 10.1002/yea.1233

687 Schindelin, J., I. Arganda-Carreras, E. Frise, V. Kaynig, M. Longair, T. Pietzsch, S.
688 Preibisch, C. Rueden, S. Saalfeld, B. Schmid, J.-Y. Tinevez, D.J. White, V. Hartenstein,
689 K. Eliceiri, P. Tomancak, and A. Cardona. (2012). Fiji: an open-source platform for
690 biological-image analysis. *Nat. Methods.* **9**, 676-682. doi: 10.1038/nmeth.2019

691 Schuberth, C., Buchberger, A. (2005). Membrane-bound Ubx2 recruits Cdc48 to ubiquitin
692 ligases and their substrates to ensure efficient ER-associated protein degradation. *Nat.*
693 *Cell Biol.* **7**, 999-1006. doi: 10.1038/ncb1299.

694 Smoyer, C.J., Jaspersen, S.L. (2019). Patrolling the nucleus: inner nuclear membrane-
695 associated degradation. *Curr. Genet.* **65**, 1099–1106. doi: 10.1007/s00294-019-00971-1

696 Smoyer, C.J., Smith, S.E., Gardner, J.M., McCroskey, S., Unruh, J.R., Jaspersen, S.L. (2019).
697 Distribution of Proteins at the Inner Nuclear Membrane Is Regulated by the Asi1 E3
698 Ligase in *Saccharomyces cerevisiae*. *Genetics* **211**, 1269–1282. doi:
699 10.1534/genetics.119.301911

700 Steglich, B., Filion, G., van Steensel, B., Ekwall, K. (2012). The inner nuclear membrane
701 proteins Man1 and Ima1 link to two different types of chromatin at the nuclear periphery
702 in *S. pombe*. *Nucleus* **3**, 77–87. doi: 10.4161/nucl.18825

703 Swanson, R., Locher, M., Hochstrasser, M. (2001). A conserved ubiquitin ligase of the
704 nuclear envelope/endoplasmic reticulum that functions in both ER-associated and Matα2
705 repressor degradation. *Genes Dev.* **15**, 2660-2674. doi: 10.1101/gad.933301.

706 Takeda, K., Mori, A., Yanagida, M. (2011). Identification of Genes Affecting the Toxicity of
707 Anti-Cancer Drug Bortezomib by Genome-Wide Screening in S. pombe. *PLoS ONE* **6**,
708 e22021. doi: 10.1371/journal.pone.0022021

709 Takeda, K., Yanagida, M. (2005). Regulation of Nuclear Proteasome by Rhp6/Ubc2 through
710 Ubiquitination and Destruction of the Sensor and Anchor Cut8. *Cell* **122**, 393–405. doi:
711 10.1016/j.cell.2005.05.023

712 Tange, Y., Chikashige, Y., Takahata, S., Kawakami, K., Higashi, M., Mori, C., Kojidani, T.,
713 Hirano, Y., Asakawa, H., Murakami, Y., Haraguchi, T., Hiraoka, Y. (2016). Inner
714 nuclear membrane protein Lem2 augments heterochromatin formation in response to
715 nutritional conditions. *Genes Cells* **21**, 812–832. doi: 10.1111/gtc.12385

716 Tatebe, H., Yanagida, M. (2000). Cut8, essential for anaphase, controls localization of 26S
717 proteasome, facilitating destruction of cyclin and Cut2. *Curr. Biol.* **10**, 1329–1338. doi:
718 10.1016/S0960-9822(00)00773-9

719 Toyama, B.H., Savas, J.N., Park, S.K., Harris, M.S., Ingolia, N.T., Yates, J.R., Hetzer, M.W.
720 (2013). Identification of Long-Lived Proteins Reveals Exceptional Stability of Essential
721 Cellular Structures. *Cell* **154**, 971–982. doi: 10.1016/j.cell.2013.07.037

722 Tsai, P.-L., Zhao, C., Turner, E., Schlieker, C. (2016). The Lamin B receptor is essential for
723 cholesterol synthesis and perturbed by disease-causing mutations. *eLife* **5**, e16011. doi:
724 10.7554/eLife.16011

725 Vembar, S.S., Brodsky, J.L. (2008). One step at a time: endoplasmic reticulum-associated
726 degradation. *Nat. Rev. Mol. Cell Biol.* **9**, 944–957. doi: 10.1038/nrm2546

727 Wach, A. (1996). PCR-synthesis of marker cassettes with long flanking homology regions for
728 gene disruptions in *S. cerevisiae*. *Yeast*. **12**, 259-265. doi: 10.1002/(SICI)1097-
729 0061(19960315)12:3%3C259::AID-YEA901%3E3.0.CO;2-C

730 Wolf, D.H., Stolz, A. (2012). The Cdc48 machine in endoplasmic reticulum associated
731 protein degradation. *Biochim. Biophys. Acta.* **1823**, 117–124. doi:
732 10.1016/j.bbamcr.2011.09.002

733 Ye, Y., Meyer, H.H., Rapoport, T.A. (2001). The AAA ATPase Cdc48/p97 and its partners
734 transport proteins from the ER into the cytosol. *Nature* **414**, 652–656. doi:
735 10.1038/414652a

736

737

738 **Figure legends**

739 **Figure 1. Bqt4 protein is degraded by the ubiquitin-proteasome system**

740 (A, B) Cells expressing GFP-Bqt4 in the *bqt3*$^{+}$ or *bqt3*Δ background were treated with
741 vehicle (+DMSO) or the proteasome inhibitor bortezomib (+BZ) for 4 h and subjected to
742 microscopic observation (A) or Western blotting (B). (A) Fluorescence microscopic images
743 of GFP-Bqt4 (upper panels); bright-field images (lower panels). Bar, 10 μm. (B) Protein
744 amounts of GFP-Bqt4 and β-actin were detected by anti-GFP and anti-β-actin antibodies,
745 respectively. Molecular weight markers are shown on the left.

746 (C, D) Cells harboring *mts3-1* in the *bqt3*$^{+}$ or *bqt3*Δ background were cultured at a
747 nonpermissive temperature (36°C) for 4 h and subjected to microscopic observation (C) or
748 Western blotting (D). (C) Fluorescence microscopic images of GFP-Bqt4 (upper panels);
749 bright-field images (lower panels). Bar, 10 μm. (D) Protein amounts of GFP-Bqt4 and β-actin
750 were detected as in (B). The asterisk in (D) indicates non-specific bands.

751 (E) Polyubiqutination of Bqt4 protein. Cells expressing GFP or GFP-Bqt4 in the *bqt3*$^{+}$ or
752 *bqt3*Δ background were treated with vehicle (+DMSO) or the proteasome inhibitor
753 bortezomib (+BZ) for 4 h. After denaturing the proteins, GFP and GFP-Bqt4 were
754 immunoprecipitated with anti-GFP antibody (IP). The precipitated proteins were detected by
755 anti-ubiquitin or anti-GFP antibodies, respectively (IB). β-actin was used as a loading
756 control. Molecular weight markers are shown on the left.

757 (F) No Bqt4 degradation by the lysosome-autophagy system. Deletion of *atg1* (*atg1*Δ) or *isp6*
758 (*isp6*Δ) was introduced into the *bqt3*Δ cells. Protein amounts of GFP-Bqt4 and β-actin in
759 these cells were detected as in (B). The asterisk indicates non-specific bands. Molecular
760 weight markers are shown on the left.

761

762 **Figure 2. Bqt4 degradation occurs in the nucleus**

763 Cells harboring *cut8-655 ts* mutation in the *bqt3*$^{+}$ or *bqt3*Δ background were cultured at a
764 nonpermissive temperature (36°C) for 4 h and subjected to microscopic observation (A) or
765 Western blotting (B). (A) Fluorescence images of GFP-Bqt4 (upper panels); bright-field
766 images (lower panels). Bar, 10 μm. (B) Protein levels of GFP-Bqt4 and β-actin were detected
767 using anti-GFP and anti-β-actin antibodies, respectively. The asterisk indicates non-specific
768 bands. Molecular weight markers are shown on the left.
769
770 **Figure 3. Bqt4 is a substrate of the Doa10 complex**
771 Bqt4 protein levels in *doa10, ubc6* and *ubc7* mutants. (A, B) Cells harboring *hrd1* (*hrd1*Δ),
772 *doa10* (*doa10*Δ) single deletion, or *hrd1* and *doa10* double deletion (*hrd1*Δ *doa10*Δ) in *bqt3*Δ
773 background were cultured at 30°C for 16 h, and then subjected to microscopic observation
774 (A) or Western blotting (B). (A) Fluorescence microscopic images of GFP-Bqt4 (upper
775 panels); bright-field images (lower panels). Bar, 10 μm. (B) Protein levels of GFP-Bqt4 and
776 β-actin were detected using anti-GFP and anti-β-actin antibodies, respectively. (C, D) Cells
777 harboring *ubc6* (*ubc6*Δ), *ubc7* (*ubc7*Δ) single deletion, or *ubc6* and *ubc7* double deletion
778 (*ubc6*Δ *ubc7*Δ) in *bqt3*Δ background were cultured at 30°C for 16 h, and then subjected to
779 microscopic observation (C) or Western blotting (D). (C) Fluorescence microscopic images
780 of GFP-Bqt4 (upper panels); bright-field images (lower panels). Bar, 10 μm. (D) Protein
781 levels of GFP-Bqt4 and β-actin were detected using anti-GFP and anti-β-actin antibodies,
782 respectively. The asterisk indicates non-specific bands. Molecular weight markers are shown
783 on the left.
784
785 **Figure 4. Bqt4 is an integral membrane protein**
786 Cells expressing GFP-Bqt4, GFP-Bqt3, or GFP-ADEL were mixed at a 1:1:1 ratio and lysed
787 by bead beating. After removing cell debris, the extracts were treated under various

788 conditions, as shown on the top. The extracts were fractionated by ultracentrifugation into
789 supernatant (S) and pellet (P), and then GFP-tagged proteins in each fraction were detected
790 by Western blotting. Molecular weight markers are shown on the left.
791
792 **Figure 5. Removal of Bqt4 requires the Cdc48 retrotranslocation complex**
793 (A) The Cdc48 mutant used in this study. Left panel: the amino acid sequence alignment
794 around the D1 and D2 domains of *S. pombe* (*Sp*) and *S. cerevisiae* (*Sc*) Cdc48. Gray and light
795 gray shades denote identical and similar amino acids, respectively (top and bottom). The
796 amino acids indicated by red (P267 and A550; correspond to red stars in the schematic
797 diagram in the middle) are both mutated in this study (P267L/A550T). Right panel: the
798 mutation sites are shown in the predicted three-dimensional structure of Cdc48 by
799 AlphaFold2 (https://alphafold.ebi.ac.uk/entry/Q9P3A7).
800 (B) Temperature sensitivity of *cdc48-P267L/A550T* mutant. Five-fold serially diluted cells
801 harboring *cdc48-P267L/A550T* mutant were spotted on the YES plate, and cultured at
802 different temperatures as indicated at the bottom.
803 (C, D) Effect of hypomorphic mutation of *cdc48* on Bqt4 degradation. Cells harboring the
804 *cdc48-P267L/A550T* mutant in the *bqt3*$^{+}$ or *bqt3*Δ background were cultured at a
805 nonpermissive temperature (16°C) for 15 h and subjected to microscopic observation (C) or
806 Western blotting (D). (C) Left panels: Fluorescence microscopic images of GFP-Bqt4 (upper
807 panels); bright-field images (lower panels). Bar: 10 μm. Right panel: the fluorescence
808 intensities in the nuclei were quantified and the relative values were plotted. The mean values
809 are plotted with standard deviation on the right panel. The number of the cells analyzed is
810 shown at the bottom. ****$p < 0.0001$ via two-tailed unpaired student's *t*-test. (D) Protein
811 amounts of GFP-Bqt4 and β-actin were detected by anti-GFP and anti-β-actin antibodies,
812 respectively. Molecular weight markers are shown on the left.

813

814 **Figure 6. The C-terminal sequence of Bqt4 is a degron**

815 The C-terminal fragments of Bqt4 are shown as a cartoon on the left. These fragments were
816 expressed as GFP-fused proteins in the *bqt3*$^{+}$ or *bqt3*Δ cells. The cells were treated with
817 vehicle (+DMSO) or the proteasome inhibitor bortezomib (+BZ) for 4 h and then observed
818 by fluorescence microscopy. Bars: 10 μm.

819

820 **Figure 7. Excess Bqt4 causes nuclear envelope deformation**

821 (A) Left panels: Fluorescence microscopic images of Ish1-GFP in *bqt4*$^{+}$ or *bqt4*Δ cells. Ish1-
822 GFP was used as a nuclear membrane marker (Asakawa et al., 2022). The cells were treated
823 with vehicle (+DMSO) or the proteasome inhibitor bortezomib (+BZ) for 4 h. The
824 images were deconvoluted using the SoftWoRx software (v7.0.0). Bar: 10 μm. Right panel:
825 The roundness index of the nucleus in these cells was measured from three independent
826 experiments (shown in blue, green, and red, respectively) and plotted as a superplot (Lord et
827 al., 2020) (right panel). The roundness index one indicates a perfect circle. The solid blue
828 circle, green triangle, and red square represent the mean value of the measurements in each
829 experiment, respectively. Black horizontal lines represent the mean value for all data that is
830 shown with standard deviation. *n* at the bottom right represents the total number of cells
831 analyzed. ****$p < 0.0001$ via two-tailed unpaired student's *t*-test.

832 (B) Fluorescence microscopic images of GFP-Bqt4 in the *bqt3*$^{+}$ or *bqt3*Δ cells. GFP-Bqt4
833 was overproduced under the *nmt1* promoter in the presence or absence of 2.5 μM YAM2 in
834 EMMG for 20 and 18 h, respectively. For comparison, *bqt4p*-GFP-Bqt4 fluorescence images
835 of cells treated with BZ (*bqt4p*+BZ) are reproduced in Figure. 1A with different display
836 scales. Bar: 10 μm.

837 (C) Growth defects by Bqt4 overproduction. GFP-Bqt4 was overproduced under *bqt4* (*bqt4p*)
838 or *nmt1* promoter (*nmt1p*) in the *bqt3*$^{+}$ or *bqt3*Δ cells. Five-fold serially diluted cells were
839 spotted on the EMMG plate in the presence or absence of thiamine for 4 days. WT indicates
840 wildtype.
841
842 **Figure 8. A model of INM protein degradation of Bqt4**
843 Excess Bqt4, with exposed TMD as a degradation signal, is recognized and ubiquitinated by
844 INM-associated E3 ubiquitin ligase complexes, including Doa10 and additional unidentified
845 E3 ligases. Ubiquitinated Bqt4 is then actively dislocated from the INM by the AAA-ATPase
846 Cdc48 complex and transferred to the nuclear proteasome for proteolysis.
847

Figure 1

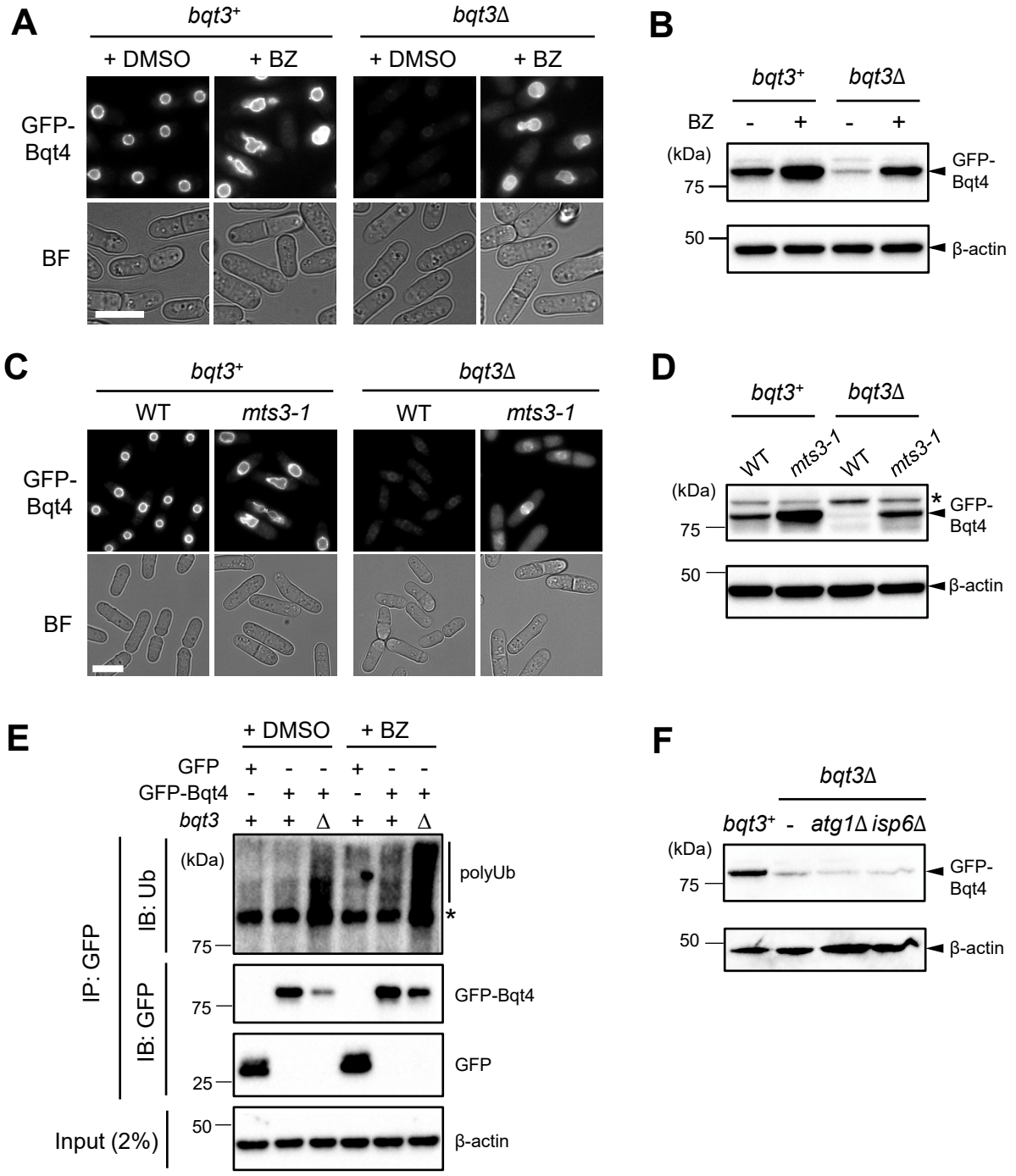
A
bqt3+
bqt3Δ
+ DMSO
+ BZ
+ DMSO
+ BZ
GFP-Bqt4
BF
B
bqt3+
bqt3Δ
BZ
-
+
-
+
(kDa)
75
50
GFP-Bqt4
β-actin
C
bqt3+
bqt3Δ
WT
mts3-1
WT
mts3-1
GFP-Bqt4
BF
D
bqt3+
bqt3Δ
WT
mts3-1
WT
mts3-1
(kDa)
75
50
*
GFP-Bqt4
β-actin
E
+ DMSO
+ BZ
GFP
GFP-Bqt4
bqt3
(kDa)
polyUb
*
75
IP: GFP
IB: Ub
IB: GFP
GFP-Bqt4
GFP
25
Input (2%)
50
β-actin
F
bqt3Δ
bqt3+
-
atg1Δ
isp6Δ
(kDa)
75
50
GFP-Bqt4
β-actin

Figure 2

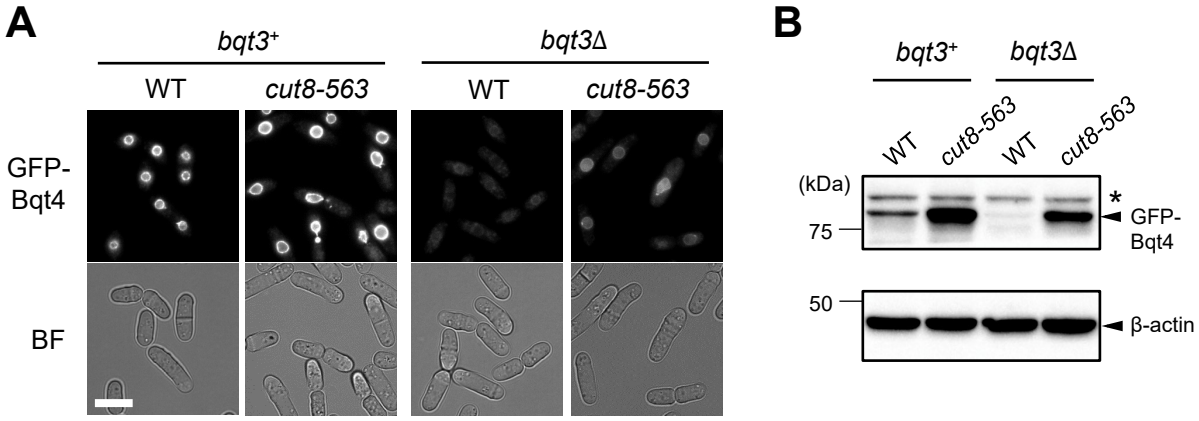
A
bqt3+
bqt3Δ
WT
cut8-563
WT
cut8-563
GFP-Bqt4
BF
B
bqt3+
bqt3Δ
WT
cut8-563
WT
cut8-563
(kDa)
75
50
*
GFP-Bqt4
β-actin

Figure 3

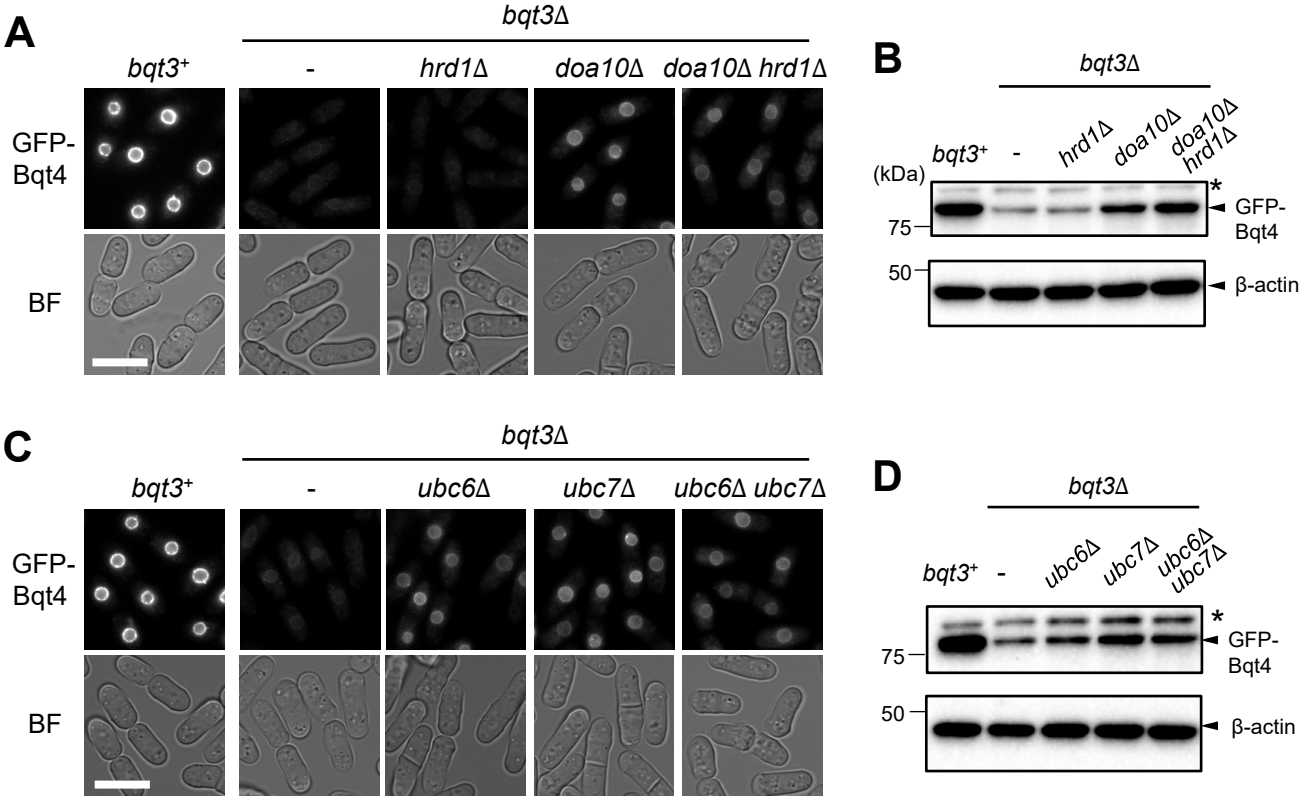
A
bqt3Δ
bqt3+
-
hrd1Δ
doa10Δ
doa10Δ hrd1Δ
GFP-Bqt4
BF
B
bqt3Δ
bqt3+
-
hrd1Δ
doa10Δ
doa10Δ hrd1Δ
(kDa)
75
50
*
GFP-Bqt4
β-actin
C
bqt3Δ
bqt3+
-
ubc6Δ
ubc7Δ
ubc6Δ ubc7Δ
GFP-Bqt4
BF
D
bqt3Δ
bqt3+
-
ubc6Δ
ubc7Δ
ubc6Δ ubc7Δ
75
50
*
GFP-Bqt4
β-actin

Figure 4

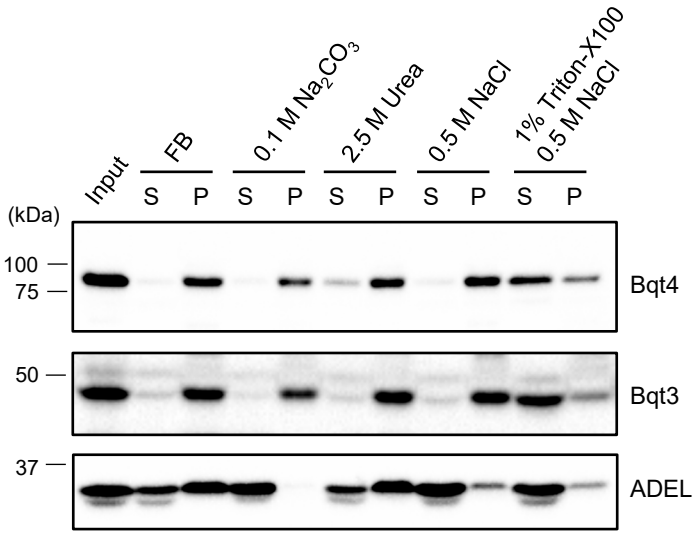
Input
FB
0.1 M Na_2CO_3
2.5 M Urea
0.5 M NaCl
1% Triton-X100
0.5 M NaCl
S
P
S
P
S
P
S
P
S
P
(kDa)
100
75
50
37
Bqt4
Bqt3
ADEL

Figure 5

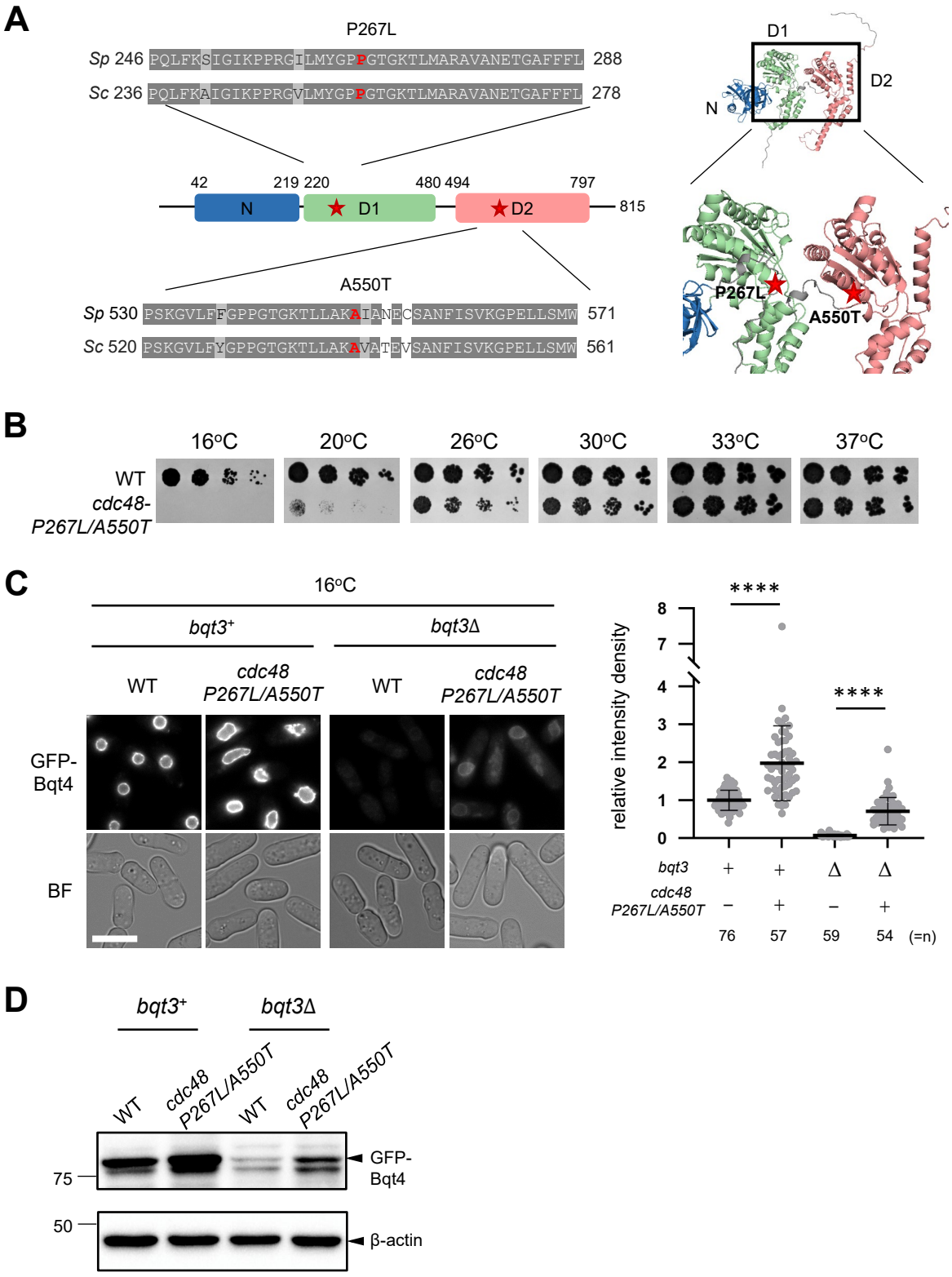
A
P267L
Sp 246 PQLFKSIGIKPPRGILMYGPPGTGKTLMARAVANETGAFFFL 288
Sc 236 PQLFKAIGIKPPRGVLMYGPPGTGKTLMARAVANETGAFFFL 278
42
219 220
480 494
797
N
D1
D2
815
A550T
Sp 530 PSKGVLFFGPPGTGKTLLAKAIANECSANFISVKGPELLSMW 571
Sc 520 PSKGVLFYGPPGTGKTLLAKAVATEVSANFISVKGPELLSMW 561
D1
D2
N
P267L
A550T
B
16°C
20°C
26°C
30°C
33°C
37°C
WT
cdc48-
P267L/A550T
C
16°C
bqt3+
bqt3Δ
WT
cdc48
P267L/A550T
WT
cdc48
P267L/A550T
GFP-
Bqt4
BF
relative intensity density
****
****
bqt3
cdc48
P267L/A550T
76
57
59
54
(=n)
D
bqt3+
bqt3Δ
WT
cdc48
P267L/A550T
WT
cdc48
P267L/A550T
75
50
GFP-
Bqt4
β-actin

Figure 6

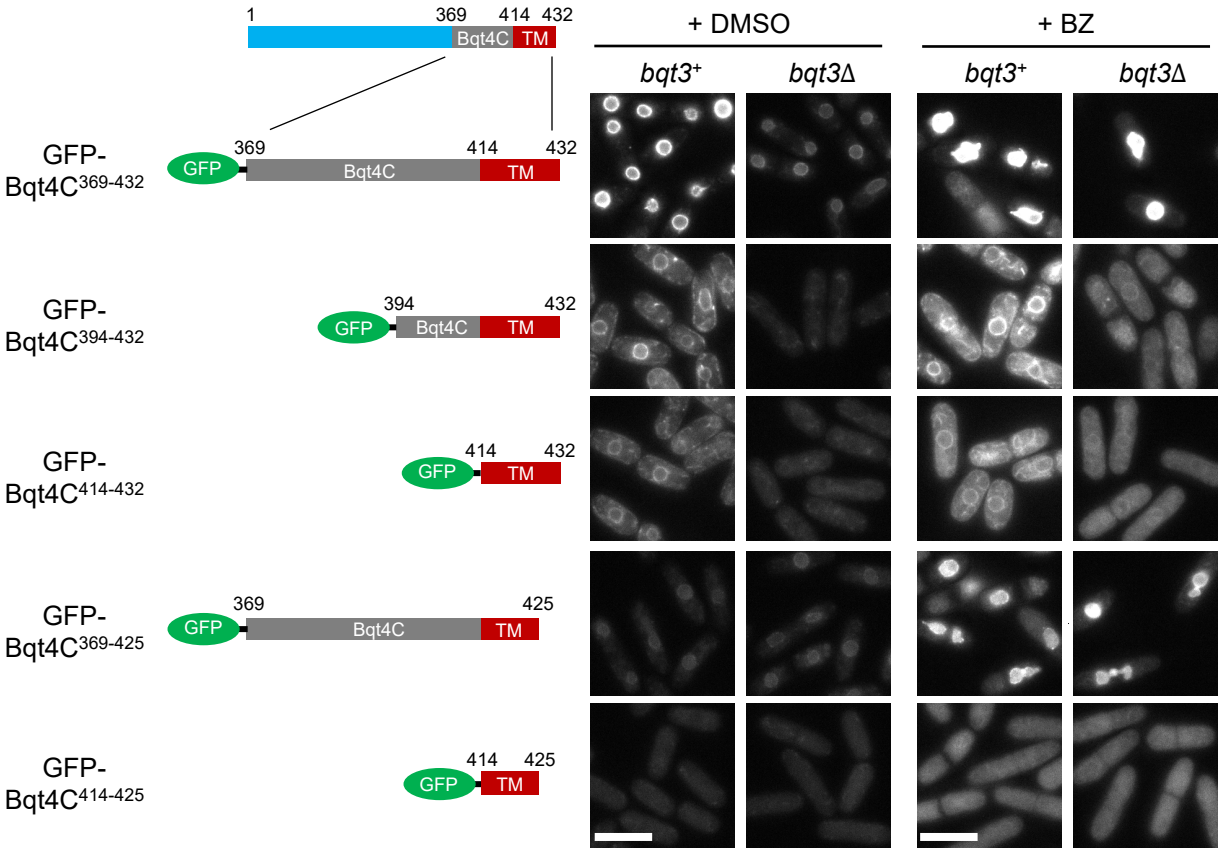
1
369
414
432
Bqt4C
TM
+ DMSO
+ BZ
bqt3+
bqt3Δ
bqt3+
bqt3Δ
GFP-
Bqt4C369-432
GFP
369
414
432
Bqt4C
TM
GFP-
Bqt4C394-432
GFP
394
432
Bqt4C
TM
GFP-
Bqt4C414-432
GFP
414
432
TM
GFP-
Bqt4C369-425
GFP
369
425
Bqt4C
TM
GFP-
Bqt4C414-425
GFP
414
425
TM

Figure 7

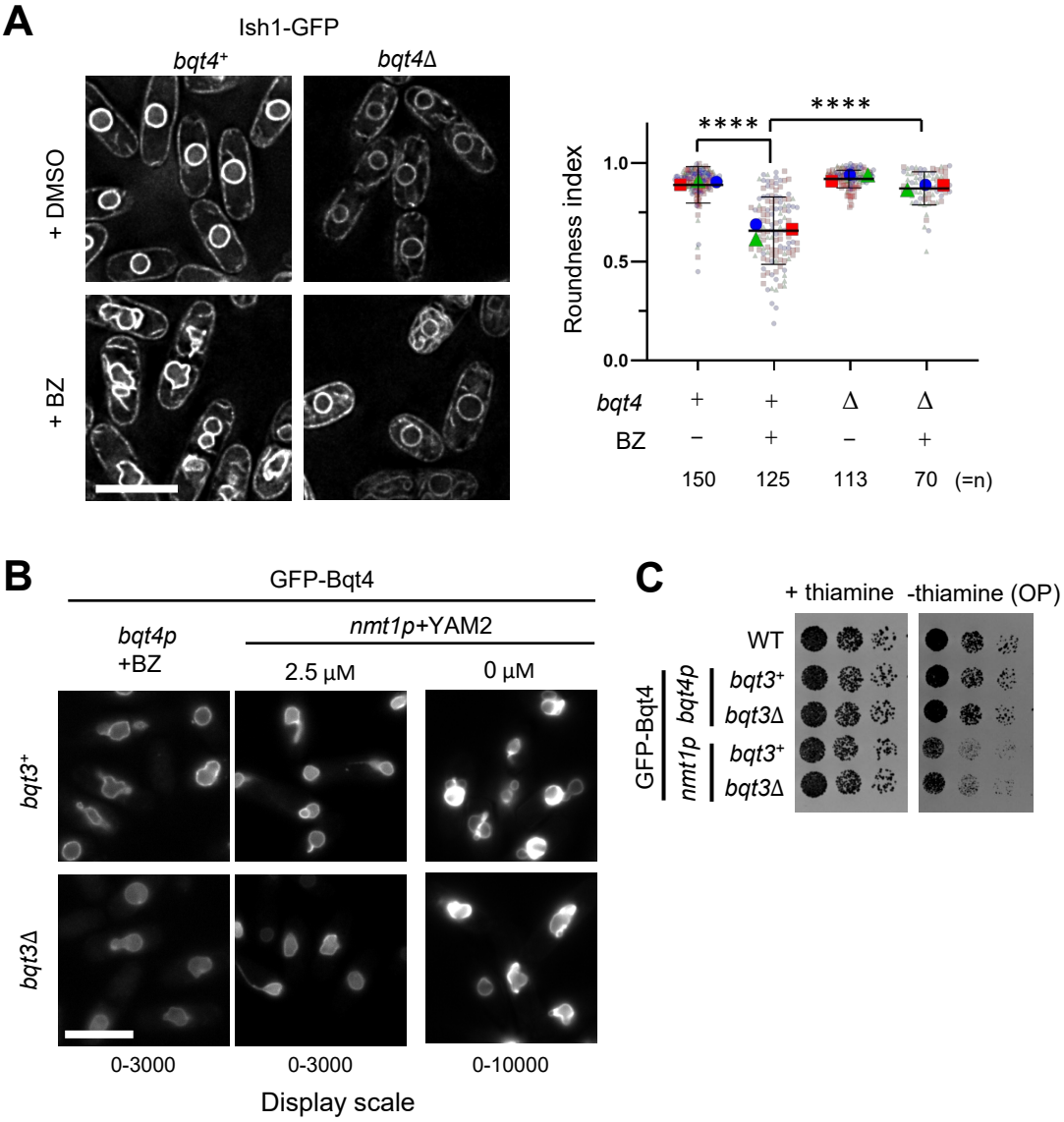
A
Ish1-GFP
bqt4+
bqt4Δ
+ DMSO
+ BZ
Roundness index
1.0
0.5
0.0
****
****
bqt4
+
+
Δ
Δ
BZ
−
+
−
+
150
125
113
70
(=n)
B
GFP-Bqt4
bqt4p
+BZ
nmt1p+YAM2
2.5 μM
0 μM
bqt3+
bqt3Δ
0-3000
0-3000
0-10000
Display scale
C
+ thiamine
-thiamine (OP)
WT
GFP-Bqt4
bqt4p
bqt3+
bqt3Δ
nmt1p
bqt3+
bqt3Δ

Figure 8

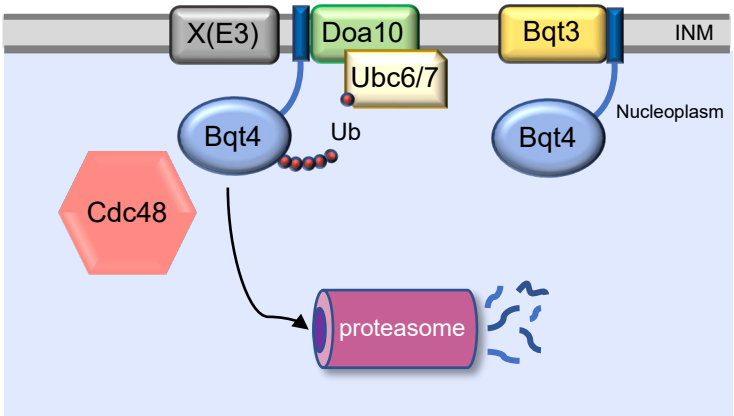
X(E3)
Doa10
Bqt3
INM
Ubc6/7
Bqt4
Ub
Bqt4
Nucleoplasm
Cdc48
proteasome

Supplementary Table 1. *S. pombe* strains used in this study

Strain	Genotype	Source	Figure
TL204	*h⁻ bqt4Δ::hph lys1⁺::bqt4p-GFP-bqt4*	This study	1A-F, 2A, B, 3A-D, 4, 5C, D 7B, C, S1, S4
TL205	*h⁻ bqt4Δ::hph lys1⁺::bqt4p-GFP-bqt4 bqt3Δ::NAT*	This study	1A-F, 2A, B, 3A-D, 4, 5C, D, 7B, C, S1, 2, 4
TL288	*h⁻ bqt4Δ::hph lys1⁺::bqt4p-GFP-bqt4 mts3-1*	This study	1C, D
TL289	*h⁻ bqt4Δ::hph bqt3Δ::NAT lys1⁺::bqt4p-GFP-bqt4 mts3-1*	This study	1C, D
H1N95	*h⁻ bqt4Δ::hph lys1⁺::bqt4p-GFP*	This study	1E
TL233	*h⁻ bqt4Δ::hph bqt3Δ::NAT lys1⁺::bqt4p-GFP-bqt4 isp6Δ::bsd*	This study	1F
TL234	*h⁻ bqt4Δ::hph bqt3Δ::NAT lys1⁺::bqt4p-GFP-bqt4 atg1Δ:: kan^r*	This study	1F
TL290	*h⁻ bqt4Δ::hph lys1⁺::bqt4p-GFP-bqt4 cut8-563*	This study	2A, B
TL291	*h⁻ bqt4Δ::hph bqt3Δ::NAT lys1⁺::bqt4p-GFP-bqt4 cut8-563*	This study	2A, B
TL215	*h⁻ bqt4Δ::hph bqt3Δ::NAT lys1⁺::bqt4p-GFP-bqt4 doa10Δ::bsd*	This study	3A, B, S2
TL219	*h⁻ bqt4Δ::hph bqt3Δ::NAT lys1⁺::bqt4p-GFP-bqt4 hrd1Δ:: kan^r*	This study	3A, B, S2
TL236	*h⁻ bqt4Δ::hph bqt3Δ::NAT lys1⁺::bqt4p-GFP-bqt4 doa10Δ::bsd hrd1Δ:: kan^r*	This study	3A, B
TL220	*h⁻ bqt4Δ::hph bqt3Δ::NAT lys1⁺::bqt4p-GFP-bqt4 ubc7Δ:: kan^r*	This study	3C, D
TL221	*h⁻ bqt4Δ::hph bqt3Δ::NAT lys1⁺::bqt4p-GFP-bqt4 ubc6Δ:: kan^r*	This study	3C, D
TL266	*h⁻ bqt4Δ::hph bqt3Δ::NAT lys1⁺::bqt4p-GFP-bqt4 ubc6Δ:: kan^r ubc7Δ::bsd*	This study	3C, D
HA1382-3D	*h⁻ lys1-131 ura4-D18 leu1-32 bqt3Δ::LEU2 aur1^r::bqt3p-GFP-bqt3*	This study	4
H1N789	*h⁻ lys1+::nmt41p-SS-GFP-ADEL*	This study	4
h-972	*h⁻*	Laboratory stock	5B, 7C
TL311	*h⁻ lys1-131 cdc48Δ:: kan^r aur1^r::cdc48p-cdc48-P267L/A550T*	This study	5B
TL306	*h⁻ bqt4Δ::hph lys1⁺::bqt4p-GFP-bqt4 cdc48Δ:: kan^r aur1^r::cdc48p-cdc48-P267L/A550T*	This study	5C, D, S4
TL307	*h⁻ bqt4Δ::hph lys1⁺::bqt4p-GFP-bqt4 bqt3Δ::NAT cdc48Δ:: kan^r aur1^r::cdc48p-cdc48-P267L/A550T*	This study	5C, D, S4
TL242	*h⁻ bqt4Δ::hph lys1⁺::bqt4p-GFP-bqt4C$^{369-432}$*	This study	6
TL243	*h⁻ bqt4Δ::hph bqt3Δ::NAT lys1⁺::bqt4p-GFP-bqt4C$^{369-432}$*	This study	6
TL246	*h⁻ bqt4Δ::hph lys1⁺::bqt4p-GFP-bqt4C$^{394-432}$*	This study	6
TL247	*h⁻ bqt4Δ::hph bqt3Δ::NAT lys1⁺::bqt4p-GFP-bqt4C$^{394-432}$*	This study	6
TL248	*h⁻ bqt4Δ::hph lys1⁺::bqt4p-GFP-bqt4C$^{414-432}$*	This study	6
TL249	*h⁻ bqt4Δ::hph bqt3Δ::NAT lys1⁺::bqt4p-GFP-bqt4C$^{414-432}$*	This study	6
TL250	*h⁻ bqt4Δ::hph lys1⁺::bqt4p-GFP-bqt4C$^{369-425}$*	This study	6
TL251	*h⁻ bqt4Δ::hph bqt3Δ::NAT lys1⁺::bqt4p-GFP-bqt4C$^{369-425}$*	This study	6
TL252	*h⁻ bqt4Δ::hph lys1⁺::bqt4p-GFP-bqt4C$^{414-425}$*	This study	6
TL253	*h⁻ bqt4Δ::hph bqt3Δ::NAT lys1⁺::bqt4p-GFP-bqt4C$^{414-425}$*	This study	6
H1N429	*h⁻ lys1⁺::ish1-GFP*	This study	7A
H1N546	*h⁺ bqt4Δ::hph lys1⁺::ish1-GFP*	This study	7A
TL206	*h⁻ bqt4Δ::hph lys1⁺::nmt1p-GFP-bqt4*	This study	7B, C
TL207	*h⁻ bqt4Δ::hph lys1⁺::nmt1p-GFP-bqt4 bqt3Δ::NAT*	This study	7B, C
TL286	*h⁻ bqt4Δ::hph lys1⁺::bqt4p-GFP-bqt4 mts2-1*	This study	S1
TL287	*h⁻ bqt4Δ::hph bqt3Δ::NAT lys1⁺::bqt4p-GFP-bqt4 mts2-1*	This study	S1
TL222	*h⁻ bqt4Δ::hph bqt3Δ::NAT lys1⁺::bqt4p-GFP-bqt4 meu34Δ:: kan^r*	This study	S2
TL224	*h⁻ bqt4Δ::hph bqt3Δ::NAT lys1⁺::bqt4p-GFP-bqt4 san1Δ:: kan^r*	This study	S2
TL225	*h⁻ bqt4Δ::hph bqt3Δ::NAT lys1⁺::bqt4p-GFP-bqt4 ubr1Δ:: kan^r*	This study	S2
TL226	*h⁻ bqt4Δ::hph bqt3Δ::NAT lys1⁺::bqt4p-GFP-bqt4 ubr11Δ:: kan^r*	This study	S2
TL227	*h⁻ bqt4Δ::hph bqt3Δ::NAT lys1⁺::bqt4p-GFP-bqt4 hul5Δ:: kan^r*	This study	S2
TL267	*h⁻ bqt4Δ::hph bqt3Δ::NAT lys1⁺::bqt4p-GFP-bqt4 dsc1Δ:: kan^r*	This study	S2
TL292	*h⁻ bqt4Δ::hph bqt3Δ::NAT lys1⁺::bqt4p-GFP-bqt4 cut9-665*	This study	S2
TL294	*h⁻ bqt4Δ::hph bqt3Δ::NAT lys1⁺::bqt4p-GFP-bqt4 ptr1-1*	This study	S2

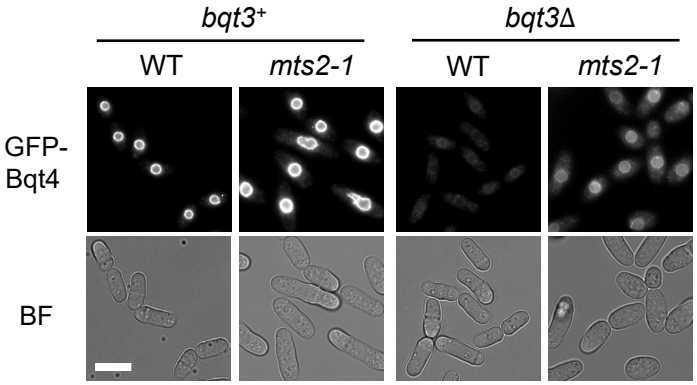

Supplementary Figure S1. The *mts2-1* mutation prevents Bqt4 degradation

Cells harboring *mts2-1* in the *bqt3*$^{+}$ or *bqt3*Δ background were cultured at a nonpermissive temperature (36°C) for 4 h and then observed by fluorescence microscopy. (Upper panels) Fluorescence images of GFP-Bqt4 (lower panels) bright-field images (BF). Bar: 10 µm.

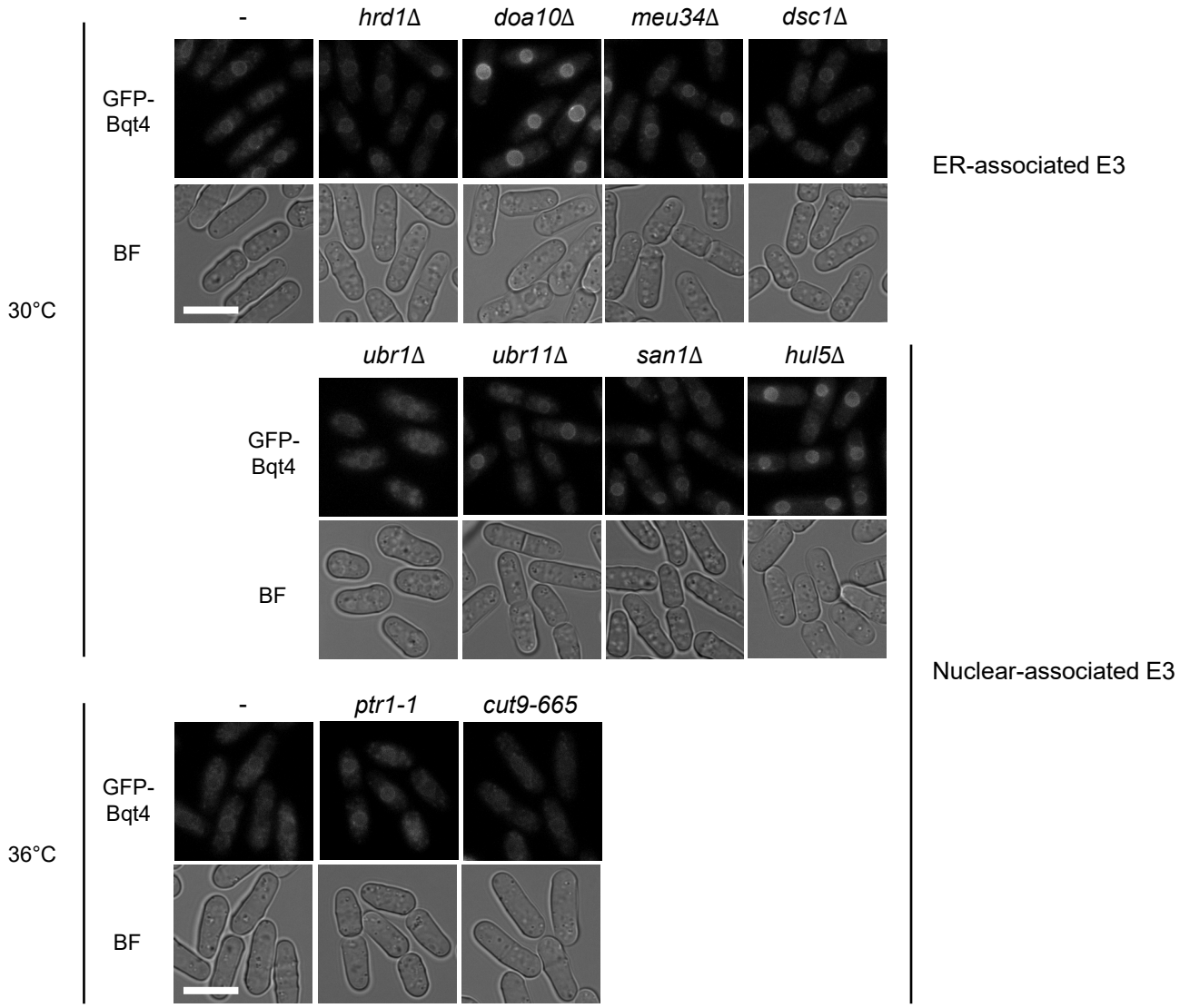

Supplementary Figure S2. Most nuclear- or ER-associated E3 ligases have a minimal role in Bqt4 degradation

Fluorescence images of GFP-Bqt4 in mutants are shown. Deletion or mutation of E3 ligases localized in the ER (*meu34*Δ, *dsc1*Δ) or functioning in the nucleus (*san1*Δ, *ubr1*Δ, *ubr11*Δ, *hul5*Δ, *ptr1-1*, *cut9-665*) was introduced in *bqt3*Δ cells expressing GFP-Bqt4. The cells were cultured at 30°C for 16 h or shifted to 36°C for 4 h for *ts* mutants and then observed using fluorescence microscopy. Bars: 10 μm.

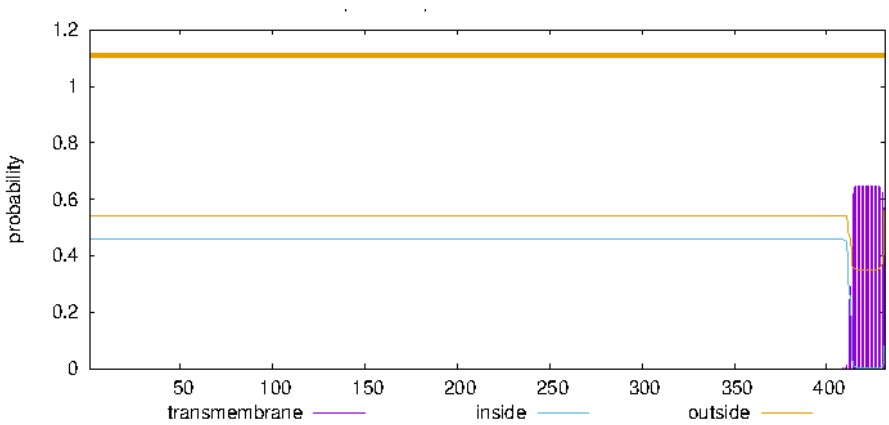

Supplementary Figure S3. Prediction of Bqt4 TMD properties

The transmembrane helices of Bqt4 were predicted by the TMHMM-2.0 prediction server (https://services.healthtech.dtu.dk/service.php?TMHMM-2.0). The horizontal and vertical axes indicate the prediction probability and amino acid residues of Bqt4, respectively.

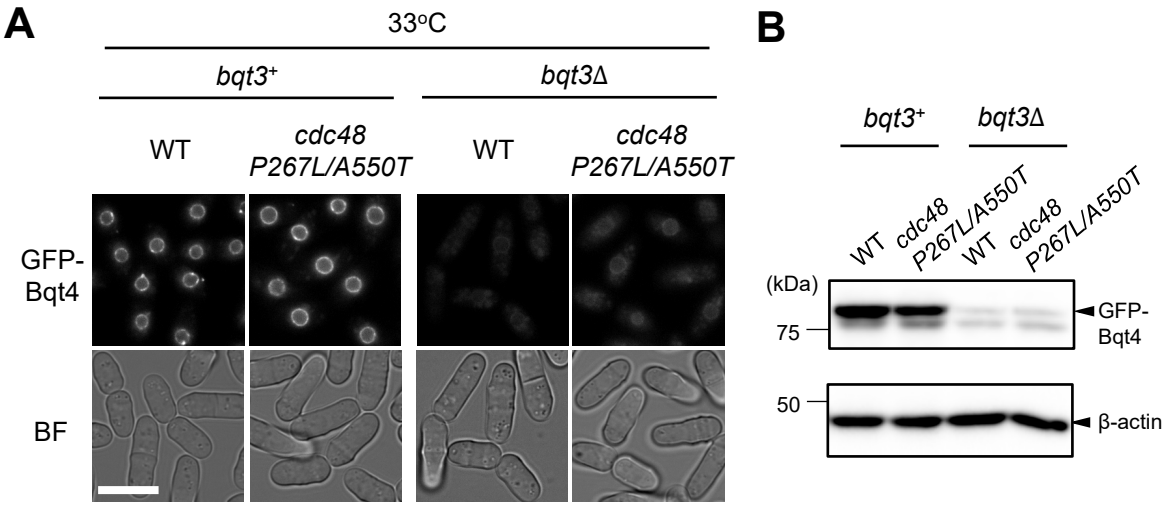

Supplementary Figure S4. Degradation of Bqt4 is not significantly affected in Cdc48 mutant at the permissive temperature

Cells harboring the cdc48-P267L/A550T mutant in the *bqt3*$^{+}$ or *bqt3Δ* background were cultured at 33°C for 15 h and subjected to microscopic observation (A) or Western blotting (B). (A) Fluorescence microscopic images of GFP-Bqt4 (upper panels); bright-field images (lower panels). Bar: 10 µm. (B) Protein amounts of GFP-Bqt4 and β-actin were detected by anti-GFP and anti-β-actin antibodies, respectively. Molecular weight markers are shown on the left.

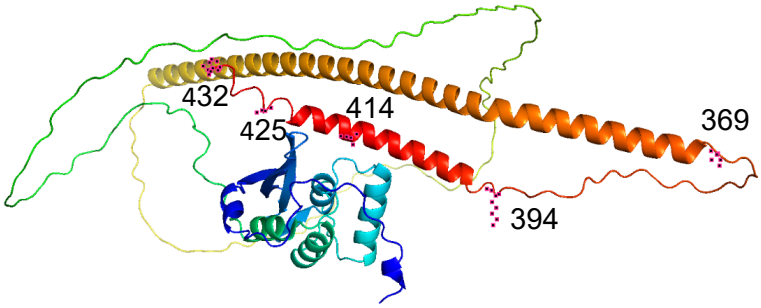

Supplementary Figure S5. Structure of Bqt4 as predicted by AlphaFold2

The three-dimensional structure of Bqt4 predicted by AlphaFold2 was obtained from the website (https://alphafold.ebi.ac.uk/entry/O60158).